Title
CHARACTERISTICS OF THE PRODUCTION OF NEUTRAL MESONS NEAR THRESHOLD IN P-P COLLISIONS

Author
Squire, Robert.

Publication Date
1955-09-13

Thesis/dissertation

UCRL 3137

UNIVERSITY OF CALIFORNIA

Radiation Laboratory

BERKELEY, CALIFORNIA

UCRL-3137

UNIVERSITY OF CALIFORNIA

Radiation Laboratory
Berkeley, California

Contract No. W-7405-eng-48

CHARACTERISTICS OF THE PRODUCTION OF NEUTRAL MESONS NEAR THRESHOLD IN P-P COLLISIONS

Robert Squire

(Thesis)

September 13, 1955

Printed for the U. S. Atomic Energy Commission

PRODUCTION OF NEUTRAL MESONS NEAR THRESHOLD IN P-P COLLISIONS

Contents

Abstract 3

I Introduction 4

II Theory 5

III Equipment and Experimental Procedure

A. Arrangement 12

B. Beam 13

C. Target 13

D. Monitor 16

E. Telescope 16

F. Collimation 20

G. Electronics

1. Schematic arrangement 21

2. Specific components 24

IV Experimental Results 34

V Analysis of the Data

A. Monitor Calibration 34

B. Beam Energy Measurements 34

C. Gamma Telescope Efficiency 36

D. Background and Subtraction 38

E. Meson Decay: Spectra 45

F. Solid Angles and Transmission Factor 46

G. Folding Operations and Calculation of Cross Sections . 51

VI Results

A. Cross Section versus Energy 55

B. Angular Distribution 55

C. Comparison with Other Experiments 58

D. Summary and Extensions 58

Appendix

A. Calculation of Photon Spectra 61

B. Calculation of Cross Sections 67

Acknowledgments 69

Bibliography 70

CHARACTERISTICS OF THE PRODUCTION OF NEUTRAL MESONS NEAR THRESHOLD IN P-P COLLISIONS

Robert Squire

Radiation Laboratory
University of California
Berkeley, California

September 13, 1955

ABSTRACT

The characteristics of the production of neutral mesons in proton-proton collisions near threshold has been studied. The external beam of the Berkeley synchrocyclotron was allowed to bombard a liquid hydrogen target and the high-energy gamma rays arising from the creation and decay of π^o mesons were detected with a counter telescope. Four independent experiments, consisting of three bombarding energies at one angle, and one energy at two angles, allowed a separation of the production contributions from the various angular momentum states that can occur.

The excitation function is composed of two terms.

$$\sigma(\text{millibarns}) = 0.020\,\eta_o^2 + 0.57\,\eta_o^8 \left\{ \begin{array}{l} +\sqrt{(0.01\,\eta_o^2)^2+(0.11\,\eta_o^6)^2+(0.31\,\eta_o^8)^2} \\ -\sqrt{(0.01\,\eta_o^2)^2+(0.11\,\eta_o^8)^2} \end{array} \right. ,$$

where η_o is the maximum meson momentum in units of μc.

The angular distribution is:

$$\frac{d\sigma}{d\Omega} = \frac{1}{4\pi}\left[0.020\,\eta_o^2 \left\{ \begin{array}{l} +\sqrt{(0.01\,\eta_o^2)^2+(0.11\,\eta_o^6)^2+(0.21\,\eta_o^8)^2} \\ -\ 0.010\,\eta_o^2 \end{array} \right. \right] + \ldots$$

$$\ldots + \frac{3}{4\pi}\left[0.57 \pm .11\right]\eta_o^8 \cos^2\theta.$$

It appears from this work that the production of π^o mesons occurs principally in the P state, accompanied by two nucleons in a P state relative to one another, down to energies about 15 Mev above threshold, at which energy this production equals the production in S states.

I. INTRODUCTION

An experiment has been performed to determine the characteristics of neutral-meson production in proton-proton collisions in which the proton energy is close to meson threshold, i.e., 30 Mev or less energy available in the c.m. system after meson production. The data obtained allow a deduction of the excitation function for the process and give some indication of the angular distribution of the mesons for the laboratory-system proton energies near 330 Mev.

The requirements of isotopic spin conservation are such as to permit an analysis of all meson production by nucleon-nucleon collisions, at energies near threshold, in terms of only three fundamental cross sections.[1,2] In the notation of Gell-Mann and Watson[2] the cross section for the reaction $p + p \rightarrow p + p + \pi^o$ or $n + n \rightarrow n + n + \pi^o$ is designated σ_{11}. Other reactions can contain σ_{11} in combination with other cross sections, but the above two reactions are the only ones in which a direct determination of this quantity can be made. Further, conservation of isotopic spin,[3,4] angular momentum, and parity place certain restrictions on the possible final states of the nucleon plus meson. It is the purpose of this experiment to obtain a measure of σ_{11} for several energies, and to determine the relative contributions of the various states possible under the above conservation laws.

The experimentally detectable property associated with the neutral meson is its decay gamma rays. That this is so stems from the fact that the π^o lifetime is of the order of 10^{-15} seconds; indeed, all proofs of the existence of the π^o rest on measurements made on the gamma rays.[5,6] It is shown in Sections V-F and VII-A of this paper that there does exist a correlation between the angular distribution of the mesons and the angular distribution of the gammas. Further, because each meson emits a fixed number of gammas--two--it is possible to determine, from the intensities of photon emission at various proton bombarding energies, the meson-production rate at these various energies and to therefore determine the excitation function. Measurements of the decay gammas were made for two different angles of view, measured with respect to the proton beam, and for three different proton energies at one angle.

II. THEORY

Since the first artificial meson production at Berkeley some eight years ago, there has been an extremely rapid development of elementary-particle physics. There now exist numerous machines capable of producing mesons, and experimentation with these has led to the accumulation of many data concerning meson production and interactions. Basic understanding of these phenomena has not progressed so rapidly, however, partly because of the complexity of field-theoretical calculations, and partly because the available data are in many cases incomplete or inconclusive.

In spite of the difficulties of the fundamental approach, it has been found possible to greatly simplify the experimental data by applying various levels of phenomenlogical theories to pion reactions. In many cases this has amounted to no more than the application of some general quantum mechanical principles. In fact, by assuming that pions are produced chiefly in P-states and by treating the nucleon-nucleon interaction phenomenologically, it has been possible to explain the energy spectra and angular distribution of pions and in some cases, to predict the excitation functions for reactions.

One result of pion reaction studies has been the growing confirmation of the charge-independence hypothesis.[1,4] This theory postulates the equality of proton-proton, proton-neutron, and neutron-neutron forces when these nucleons are in equivalent states allowed by the Pauli principle. If the π meson is the "photon" of the force field in nuclear interactions, charge independence imposes certain relations among meson-nucleon interactions. These conditions, which depend on the charge of the meson and nucleon, possess no unique simplicity. They can be elegantly described through the introduction of the concept of isotopic spin. This has the advantage of utilizing mathematical techniques familiar to physicists, but other machinery could be invented that would just as adequately give formal simplicity to the interaction scheme.

We will here attempt only the briefest summary of the theoretical concepts that have been shown to be useful. There are three major assumptions we will make in the analysis of pion-nucleon interactions.

1. Charge independence is valid; i.e., isotopic spin is conserved.

2. The pion-nucleon interaction range is finite and is, in fact, of the order of the meson Compton wave length, $\hbar/\mu c$.

3. A pion-nucleon system in the state I = 3/2, J = 3/2 has an especially strong (attractive) interaction. (I is the isotopic spin quantum number.)

Before we investigate the consequences of these assumptions, we consider the fact that for the experiments that have been performed, the energy of the pion in the c.m. system of the colliding nucleons is such that the wave length $\lambda\!\!\!^{-}$ of the meson is not small compared to the range of interaction and so only a limited number of angular momenta are involved. This interaction range is expected to be not much larger than $\hbar/\mu c$. Therefore, we do not expect orbital angular momenta greater than $\ell\hbar$, where $\ell \sim \frac{1}{\lambda\!\!\!^{-}}\left(\frac{\hbar}{\mu c}\right)$, to be important. If we plot this maximum expected ℓ as a function of the c.m. energy of the meson, we have the curve shown below.

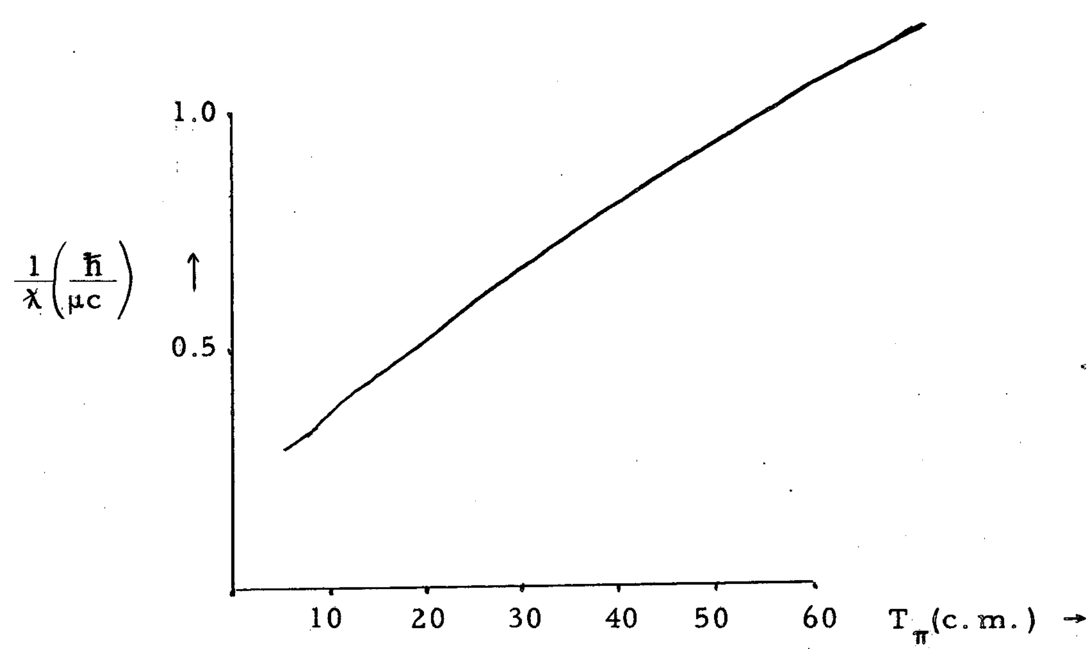

From this we see that in the energy region of 30 Mev, which is the maximum energy possible for mesons produced in p-p collisions at the Berkeley machine, we need only be concerned about angular momentum $\ell = 0$, or 1 at most. Other experiments have shown that, in fact, the state $\ell = 1$ is the most important for pion reactions.

The fact that the interaction range is limited has certain further consequences. If only one state of orbital angular momentum is important for an emitted meson, then for low energies the energy dependence of the cross section is determined.[2]

Let it be given that $T(\vec{r})$ is the scattering matrix for the emission of a particle with the space coordinate $\vec{r}$, and suppose that $T(\vec{r}) = 0$ for $r > R$, the range of interaction. If we suppose that only the angular momentum ℓ is of importance, then the amplitude for emitting a particle into a plane wave state $\phi_q(\vec{r})$(where $\vec{q}$ is the linear momentum) is

$$A_{\ell} = \int \phi_q^*(\vec{r})\, T(\vec{r})\, d^3\vec{r}.$$

Since the ℓ th partial wave varies as $\left(\frac{qr}{\hbar}\right)^{\ell}$ for $r < \frac{\hbar}{q}$, we have

$$A \propto q^{\ell} \text{ for } \frac{\hbar}{q} = \lambda\!\!\!^{-} > R.$$

The matrix element will be proportional to the square of this amplitude, or $q^{2\ell}$. We shall use this fact in the construction of our cross sections.

A consequence of the fact that only a few angular momentum states are important is that angular momentum and parity conservation will be significant in determining the possible allowable states. There is one particularly important aspect of these conservation laws. The meson is a pseudoscalar particle,[7,8] which implies that the simple emission of a meson by a nucleon must be into a state of odd orbital angular momentum. The original nucleon angular momentum ($j = 1/2$) must be conserved, so the emission must be into the $\ell = 1$, P-state. Although simple emission cannot occur alone (energy conservation), it is not unreasonable that the P-state production should predominate at low energies. This is, in fact, borne out by experience.

If we attempt to classify meson production by two colliding nucleons, at the energies considered above, we have to consider that the meson may be in an S- or P-state with respect to the mass center of the two-nucleon system, and these nucleons may be in an S- or P-state with relation to each other. For the nucleons, there will be a strong tendency for the S-state to predominate, owing to the strong attractive force in the S-state as compared to the relatively weak interaction in the P-state. This interaction will also tend to favor low nucleon energies. If we list the types of reactions accoring to their general experimental order of importance, we have:

Sp, (nucleons in an S-state, meson in a p-state)

Ss,

Pp,

Ps.

We are now ready to apply the above principles to the specific reactions that can occur to produce neutral mesons. These are seven in number:

$$\begin{aligned}
P + P &\rightarrow \pi^{+} + P + N \\
&\rightarrow \pi^{+} + D \\
P + P &\rightarrow \pi^{o} + P + P \\
P + N &\rightarrow \pi^{o} + P + N \\
N + P &\rightarrow \pi^{-} + P + P \\
N + P &\rightarrow \pi^{+} + N + N \\
N + N &\rightarrow \pi^{-} + P + N \\
&\rightarrow \pi^{-} + D \\
N + N &\rightarrow \pi^{o} + N + N
\end{aligned}$$

Under the concept of isotopic spin conservation one can express all seven of these reactions in terms of only three fundamental cross sections.[9, 10, 11] Further, it is possible to derive the excitation functions and angular distributions for these cross sections.

Let us adopt the notation of Rosenfeld[1] and others, in which σ_{ab} is the cross section for the reaction

$n + n \rightarrow \pi + n + n$,

where n = nucleon, π = meson,

for which the initial isotopic spin is a, and the final isotopic spin of the two nucleons on the right is b. Then these three fundamental cross sections are

$$\sigma_{10},$$
$$\sigma_{01},$$
$$\sigma_{11},$$

where these are listed in their experimental order of importance (magnitude). Each of these cross sections has an energy dependence of the form

$$\frac{d\sigma_{ab}}{dT_{\pi}} = \frac{2\hbar}{\hbar} \left| M_{ab} \right|^{2} \frac{dN}{dT_{\pi}},$$

where M_{ab} is the matrix element and $\frac{dN}{dT_{\pi}}$ is the density of states in phase space. These three cross sections determine the reactions as follows:

$$\sigma(PP\pi^{+}) = \sigma_{10} + \sigma_{11}$$
$$\sigma(PP\pi^{o}) = \sigma_{11}$$
$$\sigma(NP\pi^{\pm}) = 1/2\ (\sigma_{11} + \sigma_{01})$$
$$\sigma(NP\pi^{o}) = 1/2\ (\sigma_{10} + \sigma_{01})$$
$$\sigma(NN\pi^{-}) = \sigma_{10} + \sigma_{11}$$
$$\sigma(NN\pi^{o}) = \sigma_{11}$$

Of these cross sections, σ_{11} has been found to be the smallest, and has been the least studied because of this fact. It was the purpose of the experiment reported here to examine σ_{11}, measure its magnitude, and determine its excitation function. As is seen below, several combinations of meson and nucleon angular momentum may contribute to this quantity. We will attempt to calculate each contribution from the data.

The straightforward way to measure σ_{11} is through the reaction

$$P + P \rightarrow \pi^{o} + P + P.$$

The following reactions occur:

(Class Ss refers to the final state in which the nucleons are in an S-state relative to each other, and the meson is in an s-state with respect to the c.m. of the two nucleons.)

π^o Production by P-P collisions[1]

Class	Reactions	Angular distribution	Excitation function
Ss	${}^3P_0 \rightarrow ({}^1S_0 s)_0$	isotropic	$\sim 0.01\ \eta_0^{\ 2}$
Pp	${}^3P_1 \rightarrow ({}^3P_0 p)_1$ ${}^3P_{0,1,2}$ or ${}^3F_2 \rightarrow ({}^3P_1 p)_{0,1,2}$ ${}^3P_{1,2}$ or ${}^3F_{2,3} \rightarrow ({}^3P_2 p)_{1,2,3}$	$\frac{c}{3} + \cos^2\theta$	$\sim 0.2\ \eta_0^{\ 8}$
Ps	${}^1S_0 \rightarrow ({}^3P_0 s)_0$ ${}^1D_2 \rightarrow ({}^3P_2 s)_2$	isotropic	$\propto \eta_0^{\ 6}$
Sp	none	-	-

The first thing of interest from this list is that the important reaction Sp is not represented. This class, with the nucleons in the S-state and the pion in the p-state, would be expected to be the most favored. Other reactions in which this state is a contributor do show that this is an important class. For instance, in the reaction

$P + P \rightarrow \pi^+ + P + N$, the major portion of the cross section comes from just this case. The fact that it is missing here arises from the conservation laws. If the meson is pseudoscalar, the Sp class has even parity and 1 unit of angular momentum. There are no initial states for two protons that fulfill these conditions.

As pointed out above, a cross section will be enhanced if the meson and one nucleon are in an $I = 3/2$, $J = 3/2$ state. This condition cannot occur for the class Ss since there is no way for a nucleon ($j = 1/2$) to combine with a nucleon + meson with $j = 3/2$ to give 0 total angular momentum. For the classes Pp and Ps, the meson may be created in a $J = 3/2$ state with respect to one of the two P-state nucleons and be nevertheless in an s or p-state with respect to the c.m. of the nucleons.

The reaction classes Pp and Ps will tend to be depressed by the requirement that the nucleons be in a P-state relative to each other.

A priori, one cannot say whether this will be less of an influence than the enhancement due to the possibility of a (3/2, 3/2) state. Experimental evidence to date favors an excitation function that is like η_o^6 or η_o^8, which indicates that the Pp or Ps cross section is larger than the Ss.

Let the bombarding energy be such that the total kinetic energy available in the c.m. system after the reaction is T_o. Of this, an amount T is taken by the meson, and $T_o - T = E$ is taken by the internal motion of the two-nucleon system (neglecting recoil). If we express the momentum of the meson in terms of $\eta = \frac{P\pi}{\mu c}$ according to convention, and if we let η_o be the momentum of the meson (in these units) for the maximum energy T_o, we can express the differential (energy) cross sections for the various classes of reactions as the following:[2]

1. Class Ss

$$\left[\frac{d\sigma_{11}}{dT\pi}\right]_{Ss} \propto \frac{\eta\,(T_o - T)^{1/2}}{T_o - T + B'}, \qquad \left[\sigma_{11}\right]_{Ss} \propto \eta_o^2$$

The numerator is composed of a constant from the matrix element (there is no momentum dependence for the s-state), times the phase space available to the meson and nucleons. The denominator arises from the interaction of the nucleons in the s-state. B' is here the energy of two nucleons in a virtual ^1S_o state, and is considered to be essentially zero.

2. Class Pp

$$\left[\frac{d\sigma_{11}}{dT\pi}\right]_{Pp} \propto \eta^2 \cdot \eta\,(T_o - T)^{3/2}, \qquad \left[\sigma_{11}\right]_{Pp} \propto \eta_o^8$$

Here the interaction between the two nucleons is very small, or absent, and does not contribute a term in the denominator as in the above class. The numerator contains η^2 from the matrix element and η from the meson phase space. As the nucleons are emitted in a P-state, the relative momentum of the nucleons appears in the matrix element.[12]

3. Class Ps

$$\left[\frac{d\sigma_{11}}{dT\pi}\right]_{Ps} \propto \eta\,(T_o - T)^{3/2}, \qquad \left[\sigma_{11}\right]_{Ps} \propto \eta_o^6$$

Again, because the nucleons are in a P-state, there is essentially no contribution from their (weak) interaction. The meson in the s-state contributes no momentum dependence in the matrix element.

These three classes contribute to the total cross section σ_{11}. Experimental work by Marshall and Marshall[13] (η_o = 1.11) and Mather and Martinelli[14] (η_o = .62) is consistent with an excitation function of the form

$$\sigma_{11} = (.2 \text{ mb})\, \eta_o^{\ 8},$$

indicating that only the Pp class is large enough to have been detected.

It is probable that the terms due to classes Ss and Ps are not absent. An investigation of the excitation function at low energies, where the $\eta_o^{\ 8}$ term would be less predominant, ought to aid in the detection of these terms. The meson angular distribution for these classes is spherical symmetry while for the Pp class the general form including the effect of interference, is $\frac{c}{3} + \cos^2 \theta$.[1] A measurement of the meson angular distribution will therefore be an aid in separating the Pp class from the s-meson classes.

III. EQUIPMENT AND EXPERIMENTAL PROCEDURE

A. Arrangement

The experiment was performed by allowing protons to impinge on a liquid hydrogen target. The photons from the decay of the neutral mesons thus formed were detected by a gamma telescope.

The source of the protons was the 340-Mev Berkeley synchrocyclotron. The external beam from this machine was deflected by a steering magnet into a 15-foot channel in the cyclotron shielding, the last 6 feet of which consists of a tapered brass collimator of 2-inch bore. This beam then emerged into the experimental area where it was analyzed by a 12,000-gauss magnet, and was deflected here by about 20°, passed through the target, and finally went through an ionization chamber which served to measure the proton flux.

A counter array referred to below as a "telescope" was located to one side of the target and collimated so that it viewed only the region of intersection of the beam with the liquid hydrogen in the target.

The general layout is illustrated in Figs. 1 and 2, which also indicate the position of the pair of ion chambers used to measure the beam energy. These were removed during the actual running of the experiment.

B. Beam

The proton beam emerging from the brass collimator referred to above is contaminated with neutrons, which originate in the collisions of the beam edge with the collimator. If the protons are deflected with a magnet in the cave, the target may be offset so that the neutrons are prevented from striking the target. The proton beam traverses the magnet without striking the pole tips or any other material, so as to avoid any further neutron production.

For maximum-energy protons, i.e., 340 Mev, it suffices to use the beam as described above. To measure the excitation function, however, several energies are needed. These are achieved by introducing carbon absorbers in the path of the beam while it is still in the fringing field of the cyclotron. Small increments of energy can be thus quite successfully subtracted, although scattering in the absorbers reduces the beam intensity rather severely. In this experiment a rapid decrease in cross section with decreasing energy, coupled with the decrease in the beam intensity, makes it impractical to work below 320 Mev.

The beam is about 2 by 3 inches at the entrance to the target, and the target container is so constructed that at no point do the protons come closer than 2 inches from the side walls or internal structures. This is done to insure that events which take place really occur in the region of intersection of the proton beam and the liquid hydrogen target.

The measurement of the intensity and energy of the beam is described below.

C. Target

The target was a volume of liquid hydrogen 6 by 22 by 14 inches. The low cross section for π^0 production indicated that a relatively large volume would be required to achieve an adequate counting rate.

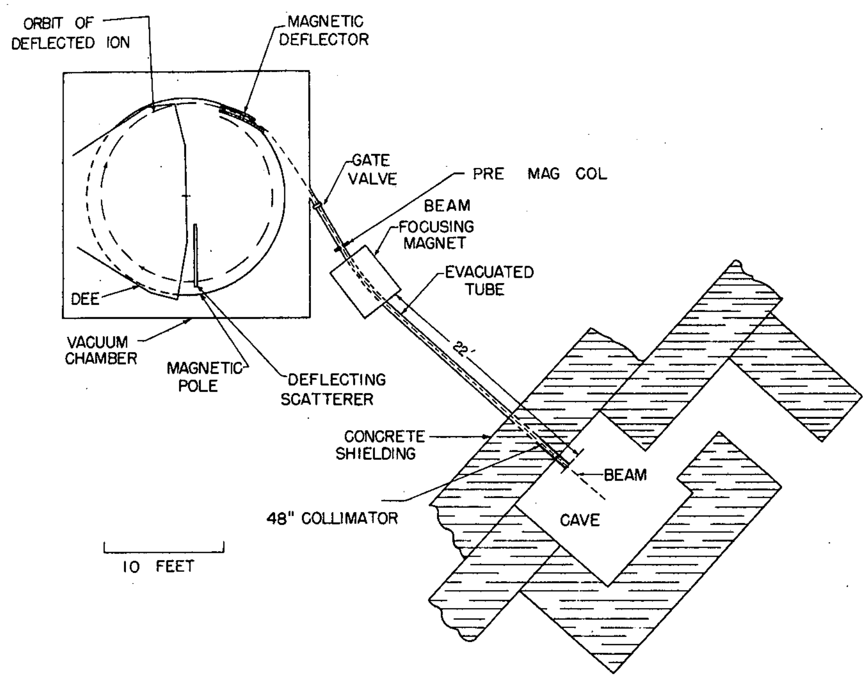

Fig. 1. General plan view of the cyclotron and experimental (cave) area.

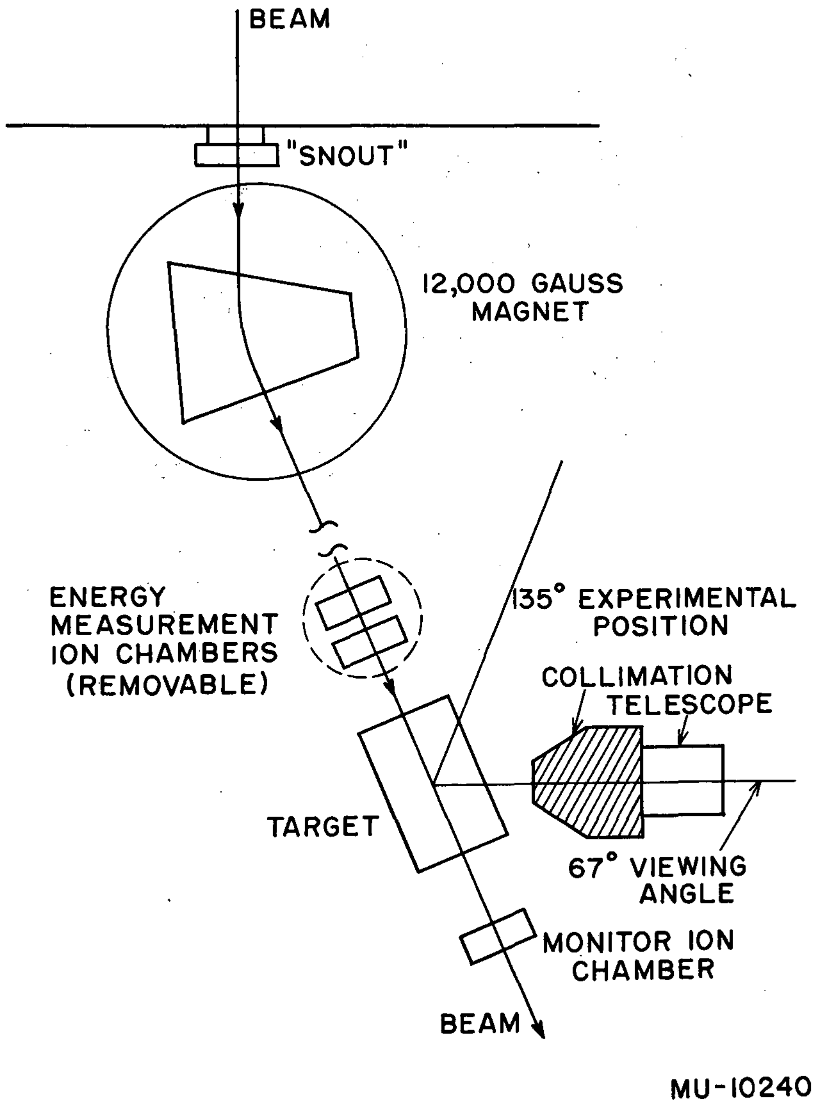

Fig. 2. Experimental arrangement in the cave area of the cyclotron, with the telescope at the 67° position.

Very little material could be tolerated in the beam path—material on which protons could produce neutrons by charge-exchange scattering, or π^- mesons which could be captured in the liquid hydrogen.

For these reasons we chose a double-walled Styrofoam target, as indicated in Fig. 3. The inner box was lined with a 5-mil vinyl bag (not indicated) to contain the liquid hydrogen in the event of the mechanical failure. The total amount of material traversed by the beam before entering liquid hydrogen was 0.175 g/cm^2.

The liquid depth was monitored by means of a simple float driving a light reed inside a graduated glass tube. After a few hours of operation, the rate of consumption of liquid hydrogen was found to be quite steady at about 4 liters per hour.

Filling was accomplished through a double-walled, evacuated, stainless steel tube. Liquid hydrogen was forced through this by applying a few pounds pressure of helium gas to a Dewar to which one end of the filling tube was sealed by a rubber sleeve.

D. Monitor

The flux of protons was measured by allowing them to pass through an ionization chamber. This was filled with helium gas at -3 pounds gauge pressure to minimize recombination.

The beam size and shape were such that the entire beam passed through the sensitive region of the ion chamber.

Calibration is described below (Section V-A).

E. Telescope

The detector, or telescope, was required to be an instrument with a high efficiency for detecting gamma rays in the presence of the very large background of ionizing radiation that one finds typical of the experimental area of the cyclotron. The design described below was the evolution of some work done to determine the optimum combination of components.

In Fig. 4, the first unit is a plastic scintillator, somewhat larger in cross section than the following units, and designed to be 100% efficient for the detection of charged particles, including those of minimum ionization. That it was so was established experimentally. This is called the "antiscintillator," and is electronically placed in

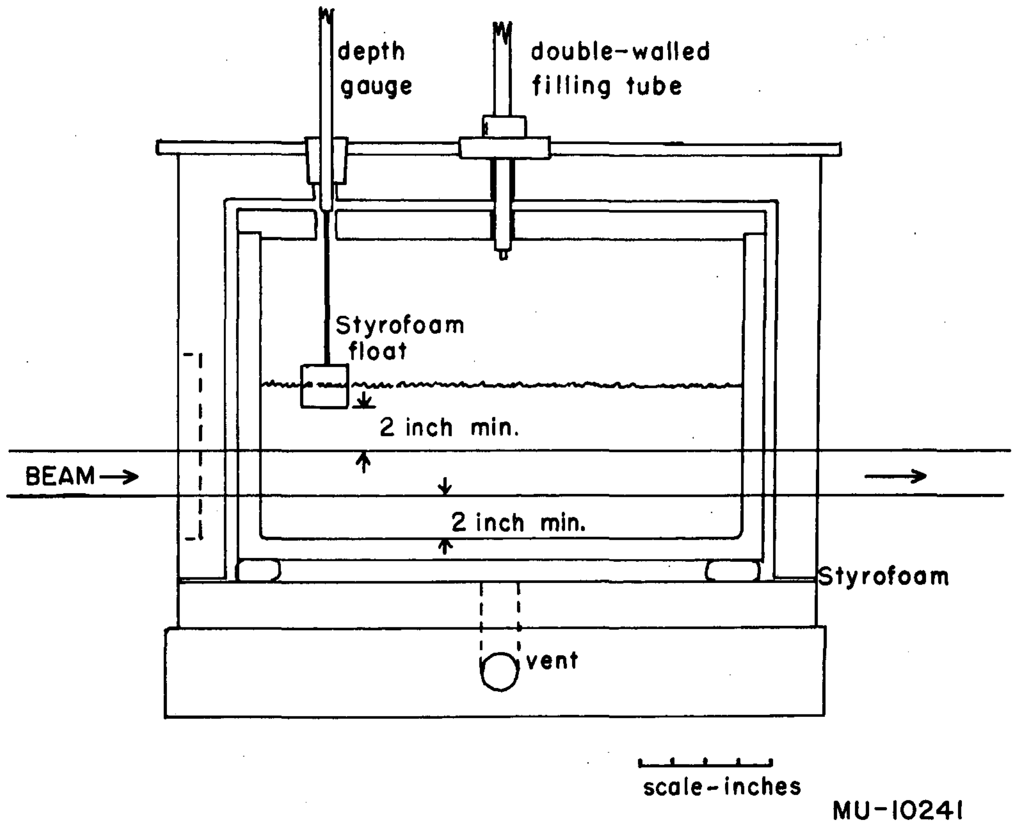

Fig. 3a. Liquid hydrogen target.

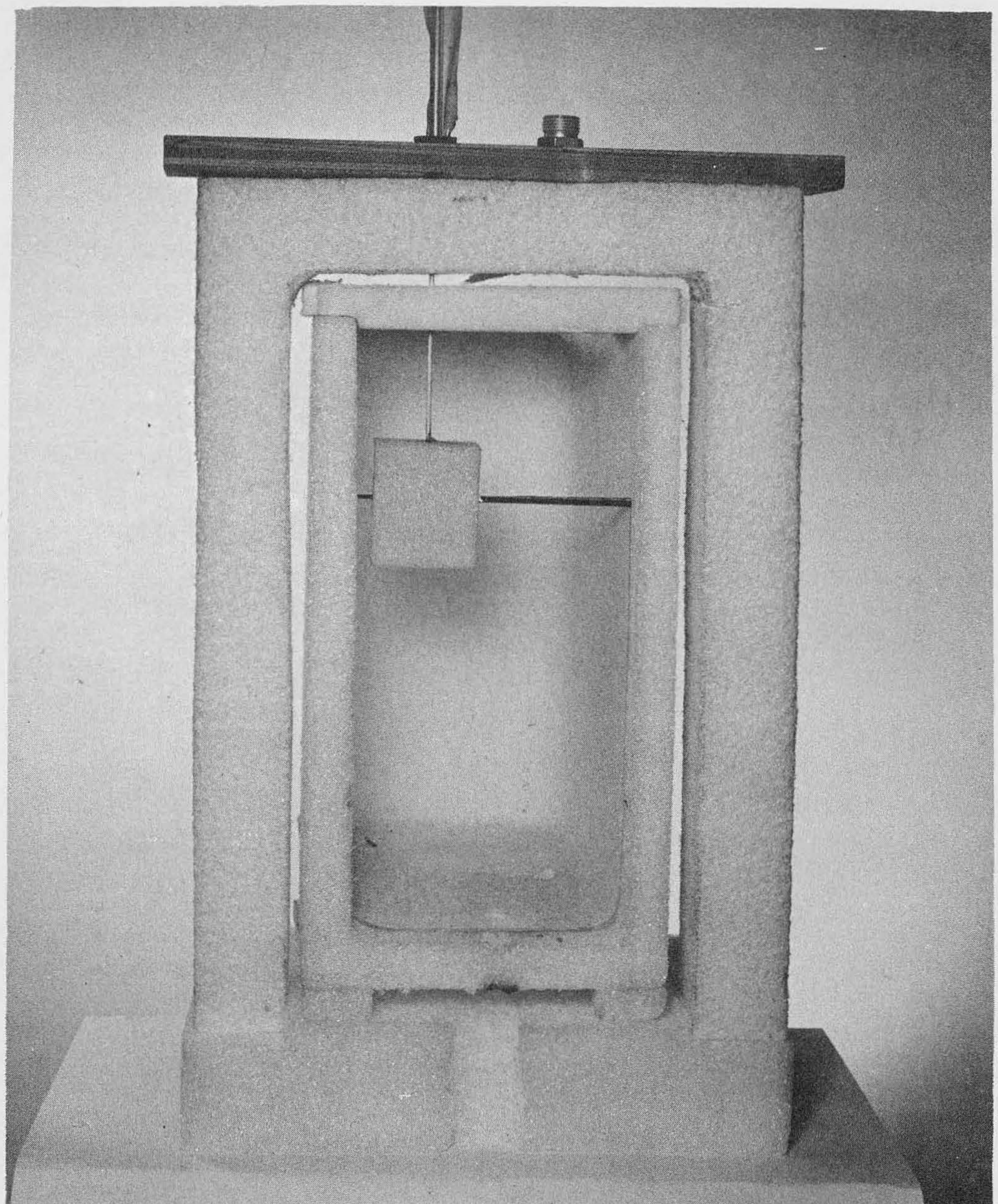

ZN-1360

Fig. 3b. Liquid hydrogen target - cross section.

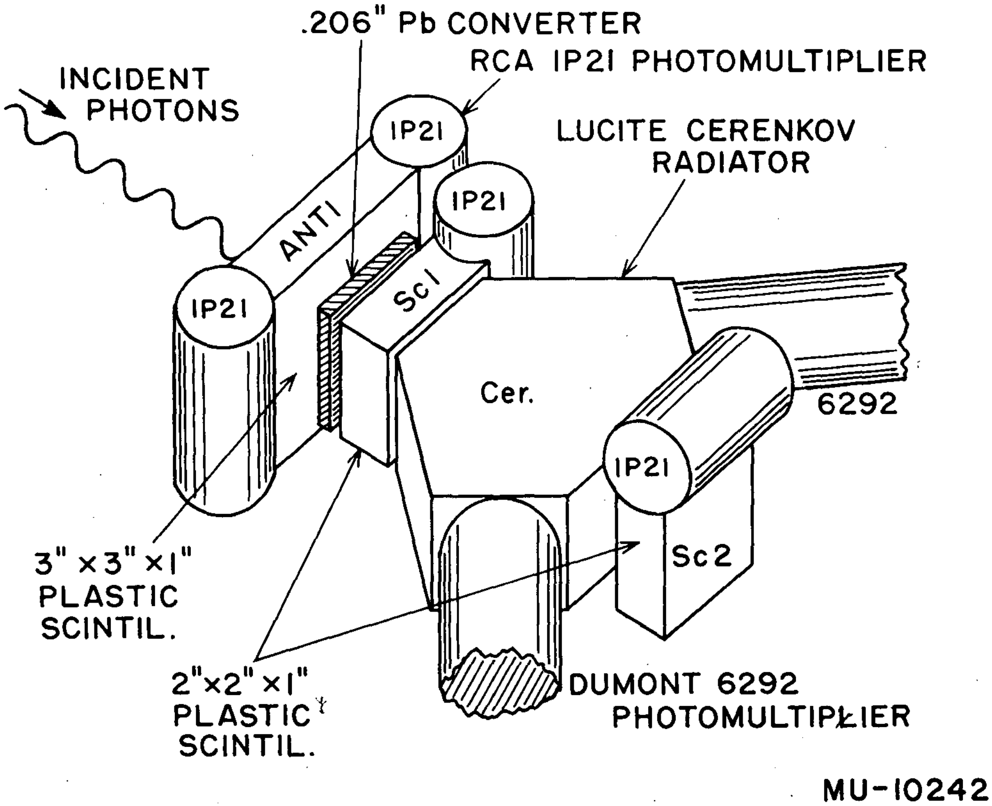

Fig. 4. Gamma telescope less all shielding.

anticoincidence with the rest of the telescope. It serves to reject charged particles incident upon the array. This is followed by a lead sheet 2 by 2 by 0.206 inches which serves to convert the gammas into electron-positron pairs. These emerge from the lead and pass successively through a 1-inch-thick plastic scintillator, a 4-inch Cerenkov counter of lucite, and another 1-inch plastic scintillator. The two scintillators are placed in electronic coincidence and serve to state that a charged particle passed through them, and hence had an energy equal to or greater than that necessary to penetrate the intervening 4 inches of lucite. The Cerenkov counter served to identify the counting event as due to a charged particle having a β approximately equal to 1. It was this counter which allowed discrimination between electrons and the very much more intense "background" of neutrons and stray radiation of other forms in the experimental area. The identification of a gamma consisted of simultaneous pulses in the two photomultipliers viewing scintillator No. 1 (Sc 1) and scintillator No. 2 (Sc 2) and in the two tubes viewing the Cerenkov radiation block, unaccompanied by a pulse from the "antiscintillator." The manifold-coincidence requirement was satisfactory in eliminating accidental counts.

The theory of Cerenkov radiation is treated by several authors. The radiation is weak, the particles emitting a few hundred photons over the visible spectrum per cm path length traversed.[15] This small light output makes it difficult to discriminate between real Cerenkov pulses and tube noise, and requires the use of either large amplification for the common coincidence circuits, or special circuits. We have used the latter approach, and employ a modified Neher bridge coincidence circuit described under "Electronics."

F. Collimation

A collimator was constructed of lead bricks which were machined for close fitting. This was 16 inches deep towards the target and contained a 2-by-2-inch hole aligned with the telescope. Enclosed by the lead was a block of beryllium 2 by 2 by 8 inches. This served to prevent low-energy charged particles from reaching the telescope, thus reducing the individual scintillator counting rates.

Figure 5 is an enlargement of the geometry of the counter, collimation, and target.

G. Electronics

1. Schematic arrangement

The circuitry associated with the gamma telescope is required to perform a logical analysis of the incoming photomultiplier pulses to determine whether they correspond to a gamma-induced event or otherwise. We recognize a gamma by its production of an electron-positron pair in the converter, and the subsequent photon production by either, or both, of these particles in their passage through Sc. 1, Sc. 2, and Cer. (see Fig. 4). The electronics then must select those events where there is a very close correspondence timewise (ideally simultaneous) between pulses from these three counters. It must reject all other combinations of pulses, and particularly those where there is an associated pulse in the "anti" counter.

Because the counters are bathed in the background radiation of the experimental area--radiation consisting primarily of low-energy neutrons--the pulse rate from any individual scintillator will be high. For this reason, the counters are paired together to operate fast-coincidence circuits. In particular, it is unnecessary to generate an antipulse for every scintillation in the anticounter, but rather only for those scintillations which are simultaneous with a pulse in one, or all, of the other counters. Similarly, we have interest in only those pulses in Sc 1 which are simultaneous with pulses in Sc 2 or the Cerenkov counter. One has as an additional source of "background" the noise pulses from the Cerenkov photomultipliers; some of these pulses are as large as the real Cerenkov pulses.

We therefore place the anticounter in fast coincidence with Sc 1; we place Sc 1 in fast coincidence with Sc 2; and we view the Cerenkov lucite block with two phototubes placed in fast coincidence with each other. At a later stage we mix the outputs of these coincidence circuits to perform our analysis.

As shown in Fig. 6, the output of the anticounter tubes is amplified by Hewlett-Packard wide-band amplifiers (200 Mc) and put into a pulse-shaping circuit to be described below. The output of

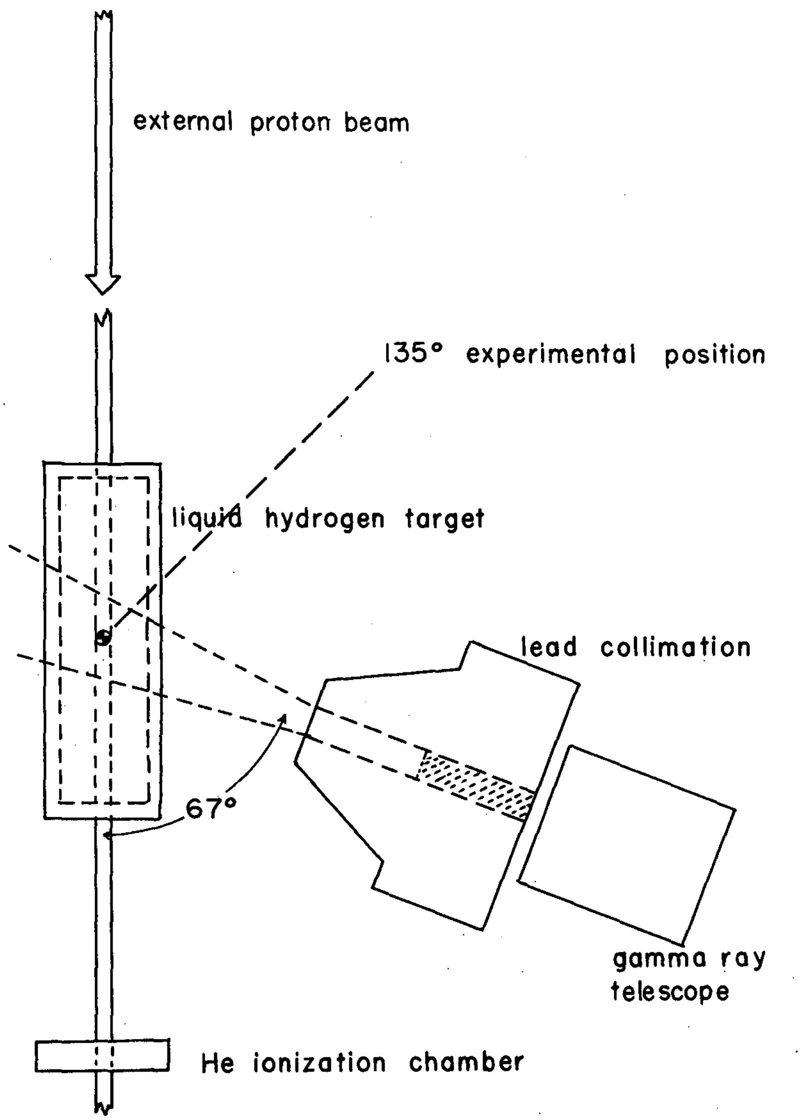

Fig. 5. Lead collimation and field of view of gamma-ray telescope with relation to target.

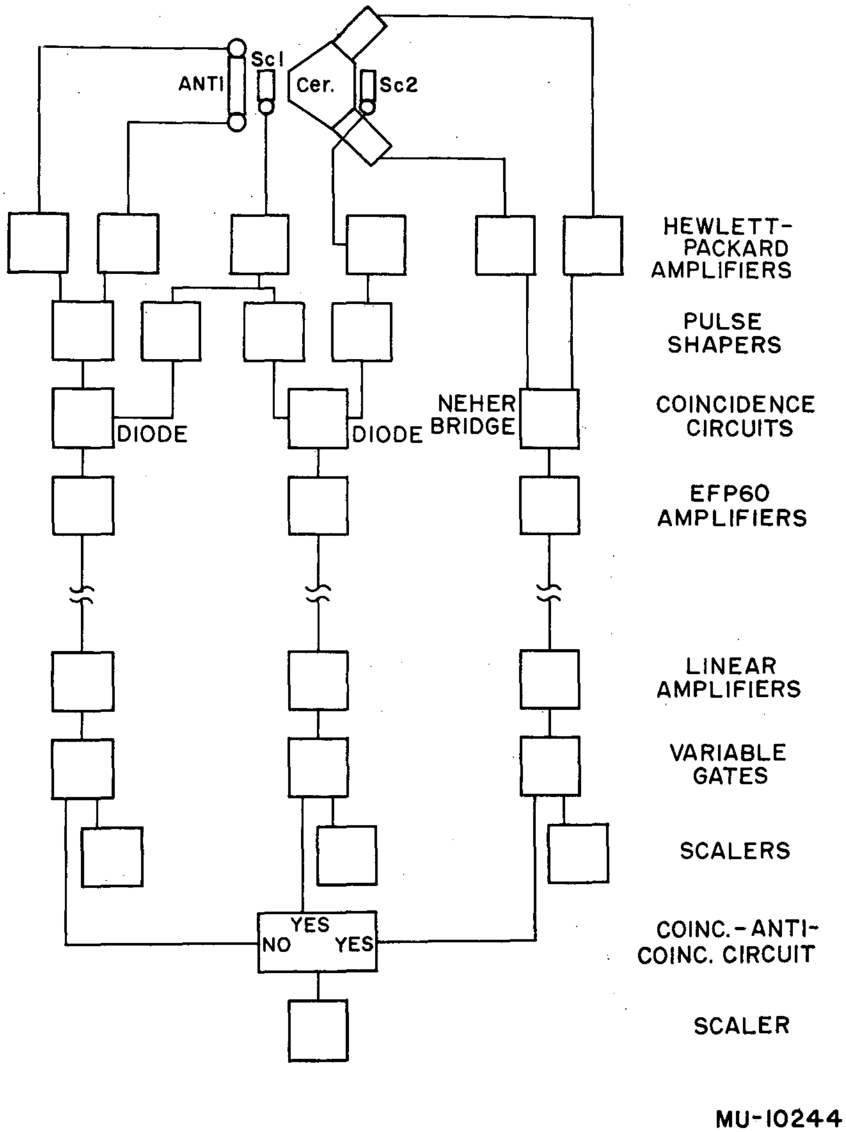

Fig. 6. Electronics block diagram.

this circuit operates one input of a crystal diode coincidence circuit.

The Sc 1 counter pulses are amplified and the signal is split, each half operating a pulse-shaping stage. The output of one of these operates the second input of the coincidence circuit receiving pulses from the anticounter. The output of the second Sc 1 pulse shaper operates an input of a second coincidence circuit. Sc 2 pulses are similarly amplified and shaped, and operate the second input of this second coincidence circuit.

The outputs of the two phototubes on the Cerenkov counter are amplified and operate the two inputs of a Neher bridge coincidence circuit.

The three coincidence-circuit outputs are each amplified by special circuits employing EFP 60 tubes, which also stretch the pulses to 1 microsecond for better matching with UCRL linear amplifiers.

This constitutes the "fast" electronics, which is operated within a few feet of the telescope. All connections are made with 197-Ω coaxial cable and care is taken that all inputs are properly terminated to prevent reflections.

The signals from the EFP 60 amplifiers are sent to the counting room on 125-Ω cable and introduced into standard equipment linear amplifiers with a band width of the order of 8 Mc. The signals then operate variable gates.

The three signals from the variable gates, one from the "Anti" plus Sc 1, another from Sc 1 plus Sc 2, and the third from the Cerenkov counter, are then mixed in a coincidence-anticoincidence circuit which responds only when there appears a pulse in the Sc 1 plus Sc 2 <u>and</u> Cerenkov outputs, but none in the anti-plus-Sc 1 input, within the one microsecond width of the variable gate pulse. The output of this circuit operates a scaler. In addition, other pulses from the variable gates operate scalers to allow monitoring of component operation.

2. <u>Specific components</u>

<u>a. Counters</u>

The scintillation counters consisted of blocks of plastic scintillator material. This is a solid solution of terphenyl, with tetraphenyl-butadiene frequency shifter, in polystyrene. The light output is about 40% that of anthracene; it has a peak frequency of 4500 A°, and a decay time of 4 millimicroseconds. The gamma-pair-production length is of the order of 50 cm.

Each block of scintillator is viewed by one RCA 1P21 photomultiplier, with the exception of the "Anti," which is viewed by two. The outputs are taken from the collector and this negative pulse is fed directly into a 197-Ω cable.

The construction of a typical counter, as well as its normal operation, is indicated in Fig. 7.

b. Cerenkov counter

The Cerenkov counter is formed from lucite and is 4 inches long in the particle traversal direction. The two DuMont 6292 tubes view this at an angle such that the Cerenkov light cone is incident normal to the faces of the tubes. The joint between the lucite and the glass is made optically good by filling the intervening space with mineral oil. The tubes are shielded from stray magnetic fields by 1/16-inch mu-metal. See Fig. 8.

c. Fast amplifiers

Commercial Hewlett-Packard model 460A amplifiers were used between the photomultipliers and the pulse-shaping circuit. The band width of these is about 200 Mc, which increases the rise time of the photomultiplier pulses to about 4 or 5 mμsec.

d. Pulse-shaping circuits

Figure 9 is a schematic of the circuit used to modify the phototube pulses. An 18-inch clipping stub shortens the pulse to 3×10^{-9} second, thus equalizing the "decay" time of pulses of various amplitudes. Each minimum-ionization scintillation pulse drives the tube to cutoff, thereby limiting the output pulse size. Where needed, pulses can be added together. A comprehensive description of this, the following crystal diode coincidence circuit, and the EFP 60 amplifier can be found in UCRL-1880.[16]

e. Coincidence circuits used in conjunction with pulse-shaping circuits

These consisted of crystal diode circuits, with a Garwin-type

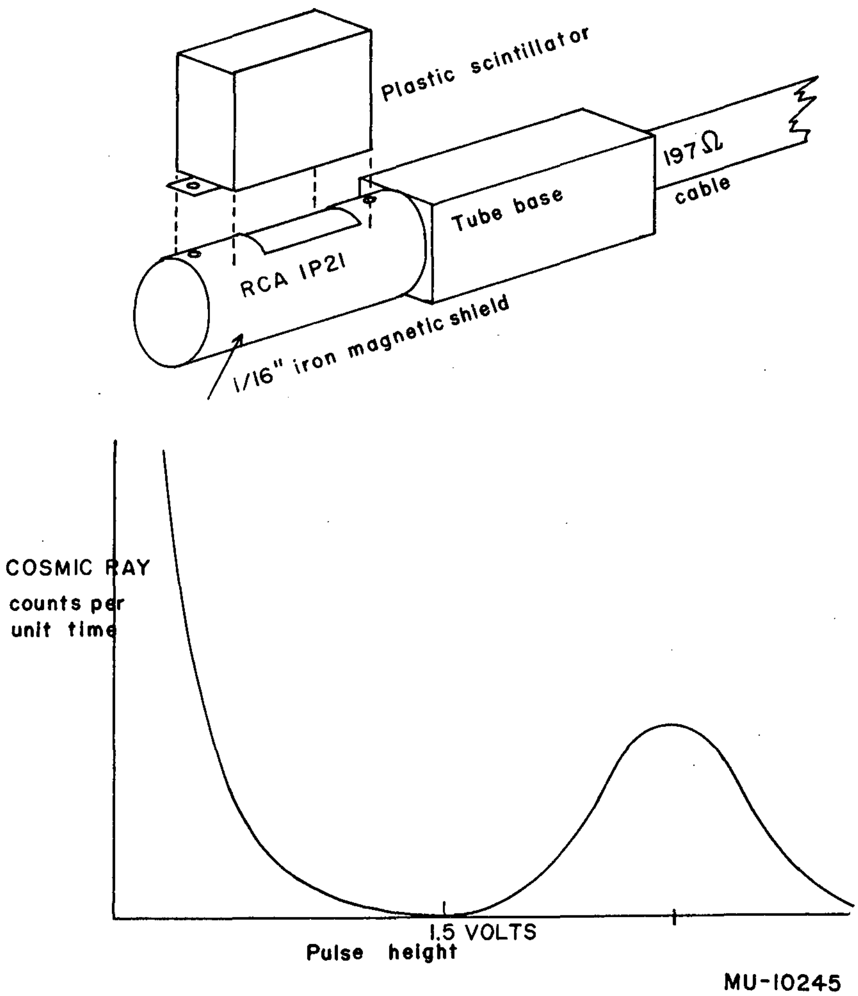

Fig. 7. Typical scintillation counter and cosmic ray differential pulse height distribution for operation with 1700 volts applied to photomultipliers.

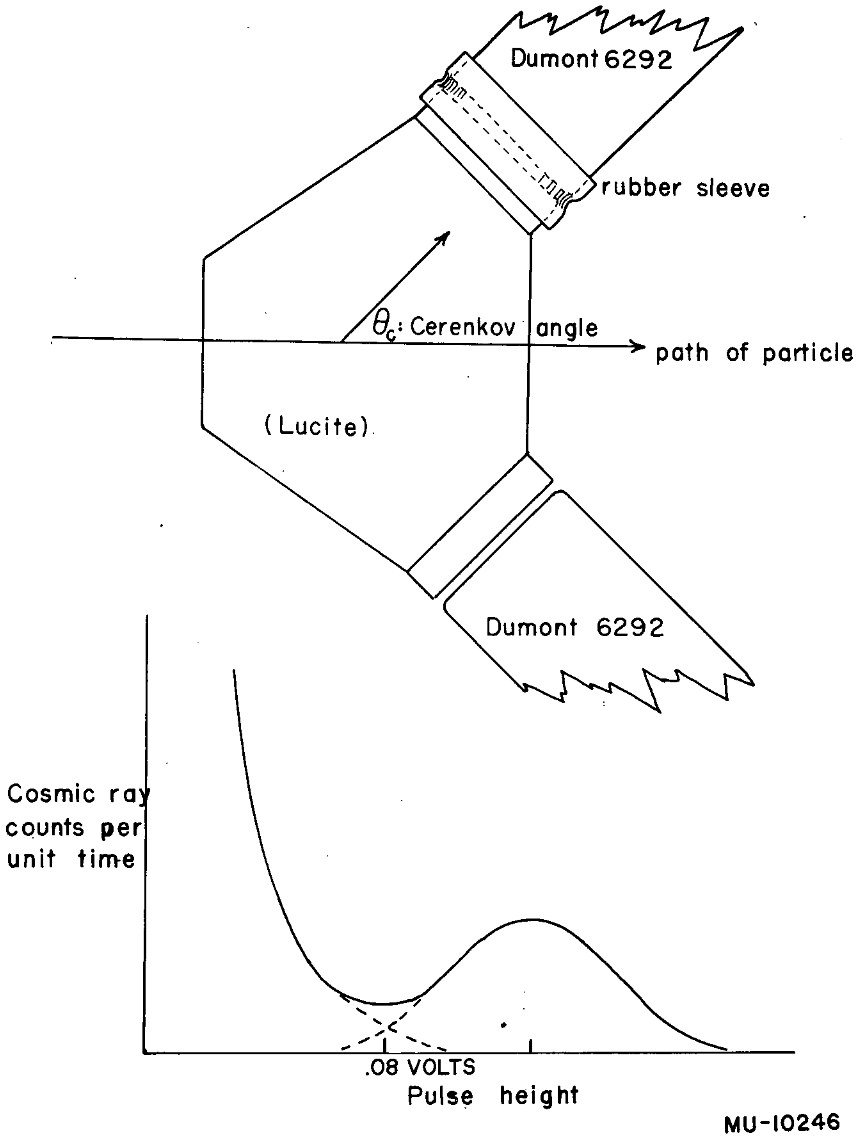

Fig. 8. Cerenkov counter and cosmic ray differential pulse height distribution for operation with 1700 volts applied to photomultipliers.

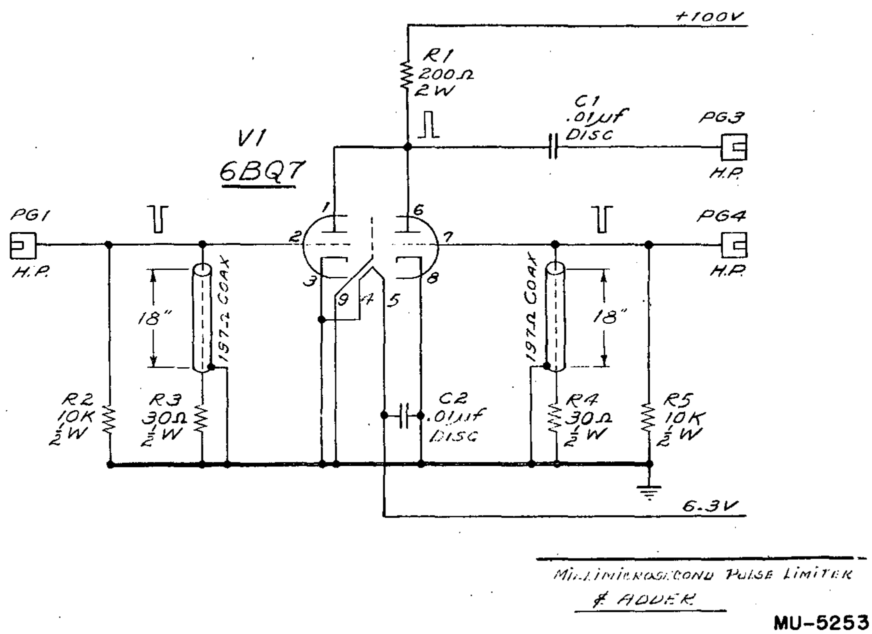

Fig. 9. Schematic of the pulse-shaper circuit.

plate clamp, and an additional discrimination diode clamp as described by Madey.[16] The circuit diagram is shown in Fig. 10. These units were found to operate exceptionally well on limited pulses, giving discrimination ratios (pulse size for coincident pulses to pulse size for single input) of the order of 50:1. Figure 11 is a plot of their absolute efficiency versus time delay in the input of either pulse. The resolution is 4 to 5 mμsec.

f. <u>EFP 60 amplifiers</u>

Because the coincidence circuit outputs are too fast to operate standard Radiation Laboratory counting equipment and too small to be easily distinguished from noise pickup in the signal cables, these outputs are stretched and amplified in a special circuit, shown in Fig. 12, employing EFP 60 secondary emission tubes. The output of this circuit is of the order of one microsecond and is matched to the 125-Ω signal-transmission lines.

g. <u>Bridge coincidence circuit</u>

This is a variation of the Neher bridge circuit which is capable of operating on very small input pulses. Figure 13 is a diagram of the circuit used for positive signals of approximately 0.5 volt. The requirement was made that the polarity of the output signal for a single input pulse be opposite to that for coincident pulses. The starred 5K resistor and crystal diode in the cross feed of the network was empirically determined so as to give this condition. The 6BQ7A acts as a difference amplifier, while the 6AK5 below it is a constant-current device. The following tubes are an amplifier and a cathode follower. A crystal diode is placed in the input to the last stage to limit pulses of the wrong (+) output polarity. This circuit has a resolution time of 3 mμsec. Normally, however, it was used in conjunction with Hewlett-Packard amplifiers which degraded this resolution time to the width of the incoming pulses, about five mμsec. The discrimination ratio was about 80:1.

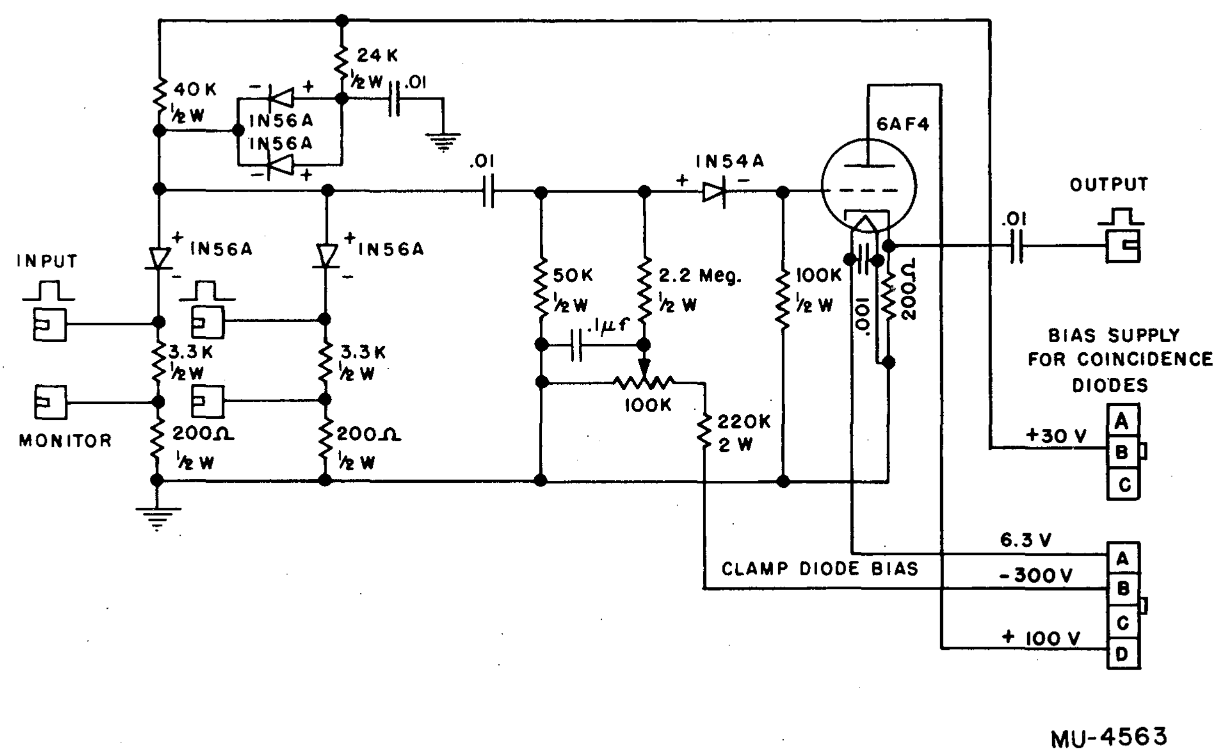

Fig. 10. Schematic of the crystal-diode coincidence circuit.

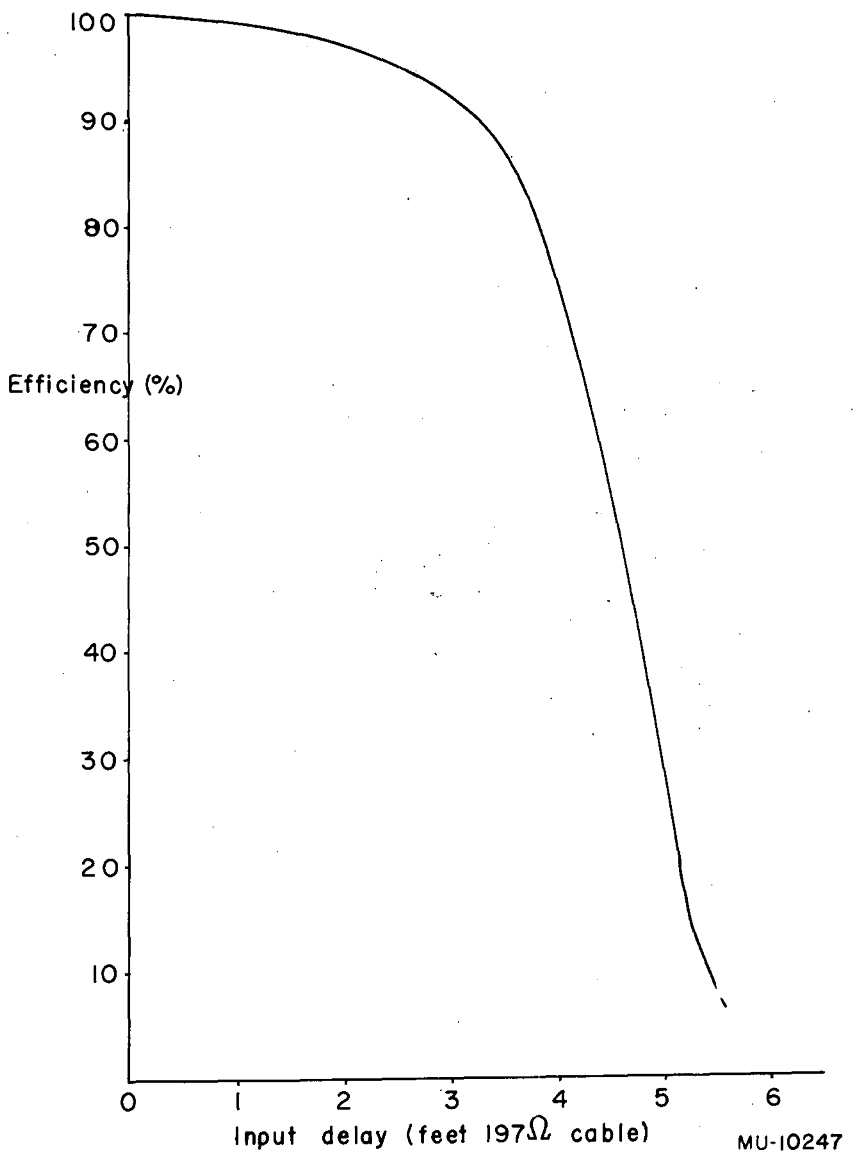

Fig. 11. Efficiency of a crystal-diode coincidence circuit for two pulses vs time delay between pulses.

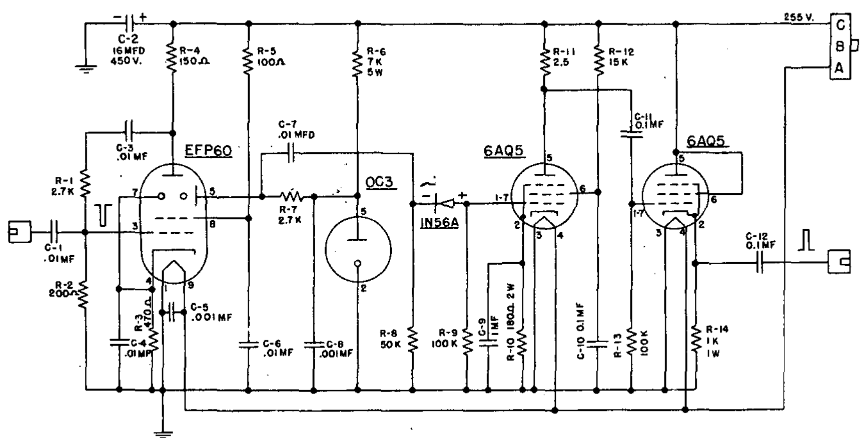

MU-6024

Fig. 12. Schematic of an EFP 60 amplifier.

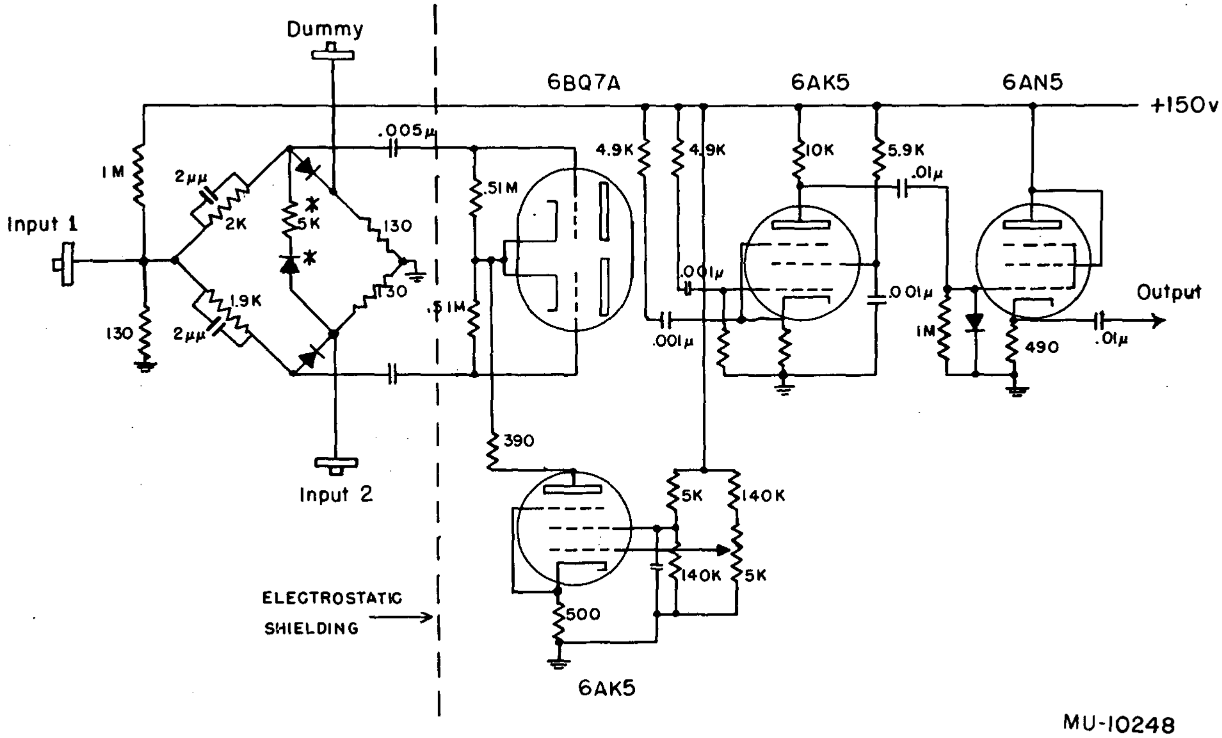

Fig. 13. Neher Bridge coincidence circuit for positive input pulses.

IV. EXPERIMENTAL RESULTS

The data, reduced to counts per proton incident on the active target volume and corrected by the subtraction procedure of Section V-D, are the following:

Run	Lab. Angle	Proton Energy (Mev)	cts per proton x 10^{10}
1	67^o	329	$2.33 \pm .10$
2	67^o	319.5	$1.36 \pm .11$
3	67^o	314.5	$1.03 \pm .11$
4	135^o	329	$0.57 \pm .03$

The monitor calibration and beam-energy determination are described in the next section under heading V-A and V-B respectively.

V. ANALYSIS OF DATA

A. Monitor Calibration

The proton flux was measured with an ion chamber, which was calibrated with a Faraday cup. In this calibration the beam was allowed to pass through the chamber and into a copper block that stopped the protons. The charge collected by the cup was a direct, absolute measure of the number of protons incident upon it. The charge collected by the ion chamber per proton traversal can then be calculated and this information used to determine the number of protons incident upon the target during the experiment. This process was repeated for the various energies and at the various beam levels used in the experiment. The results, in charge collected by the ion chamber divided by charge collected by the Faraday cup for various proton energies, is given in Fig. 14.

B. Beam Energy Measurements

The energy of the cyclotron beam is not a constant, but varies for different operating conditions by as much as 5 Mev. Because the cross section that was to be measured was a sensitive function of the energy, an exact value of this energy was needed. To determine this, two ion chambers were used, between which copper absorbers were placed to trace out the Bragg curve. An example of the results of this

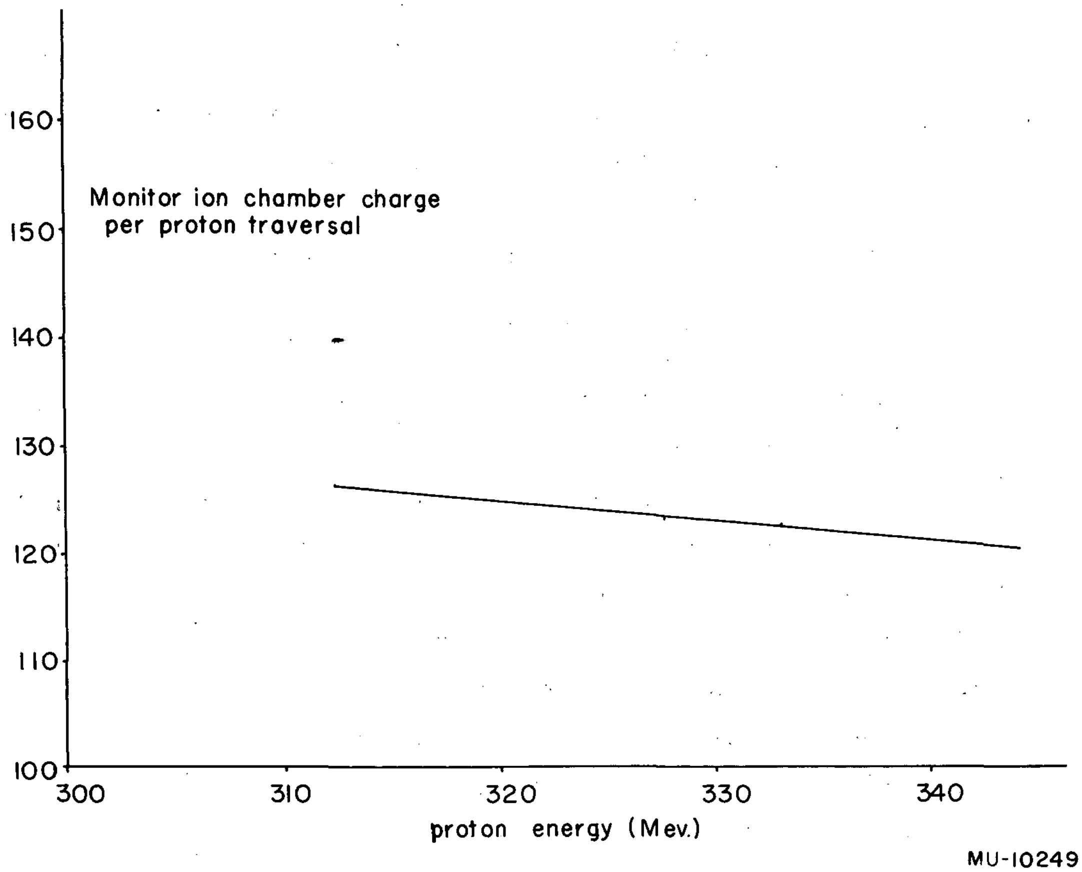

Fig. 14. Response of monitor ionization chamber for protons of various energies.

procedure is given in Fig. 15, which shows the energy in this case to correspond to 90.4 g/cm^2 Cu. For our standard of range-energy relations we took the tables of Rich and Madey, UCRL-2301.[17] The criterion of 82% peak height comes from the work done by Mather and Segrè,[18] in which they show that this choice gives an energy value that is independent of energy spread (if Gaussian) and is the choice upon which the above tables have been contructed. In the experiment, the protons traversed 1.95 g/cm^2 of liquid hydrogen, on the average, in reaching the sensitive region of the target. This degraded their energy by several Mev. The results are:

RUN	T (cyclotron) (Mev)	T (bombarding) (Mev)
1	342.5	329.0
2	333.3	319.5
3	327.5	314.5
4	342.5	329.0

C. Gamma Telescope Efficiency

The determination of the efficiency of the telescope for the detection of gamma rays of different energies was accomplished in the following manner. First, an experimental test was made of the ability of electrons of various energies to penetrate converters of lead of various thicknesses from 0 to 0.25 inch, pass through, and register in scintillator No. 1, scintillator No. 2, and the Cerenkov counter. These electrons were obtained by allowing the bremsstrahlung beam of the Berkeley synchrotron to create a spectrum of electrons in a thin converter, analyzing these electrons in a magnet, and selecting the desired energy. Upon emerging from the magnet, they are caused to pass through an auxiliary electron monitor consisting of two plastic scintillators, each 3/8 inch thick. (Fig. 16). In area, these scintillators are 1/9 the area of the 2-by-2-inch converter of the main telescope, so as to allow for exploration of various regions of this converter. The number of electrons through the monitor is the number of electrons incident on the telescope in the area covered by the monitor, and the number of events in which the telescope and the

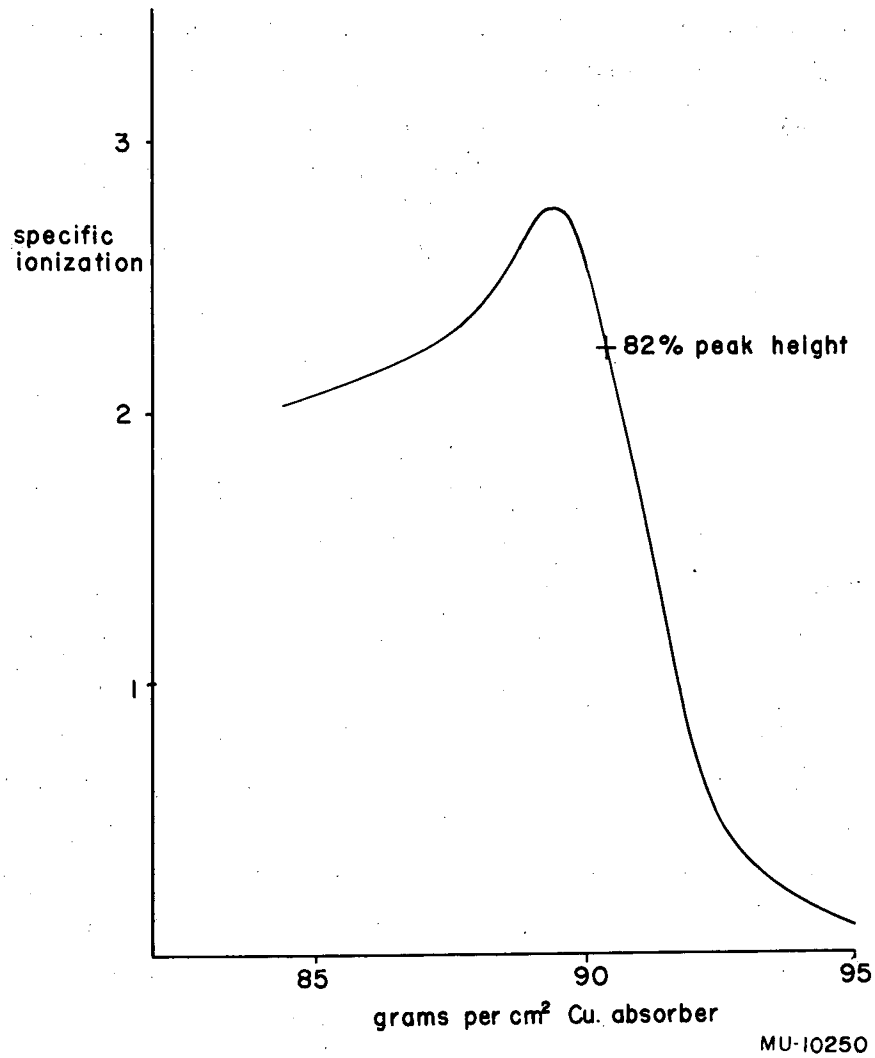

Fig. 15. Typical Bragg ionization curve as found in the determinations of the proton bombarding energies.

monitor pulses occur in coincidence is the number of "successful" traversals of the telescope by the monitored electrons. The efficiency for counting electrons is then

$$\text{Eff.} = \frac{\text{No. of coincidences (monitor + telescope)}}{\text{No. in monitor}} \times 100\%.$$

(Fig. 17)

The efficiency used below is the average of the weighted efficiencies for the detection of electrons incident on various areas of the 2-by-2-inch converter. The arrangement of this method, and the electronics employed, are shown in Fig. 16.

Finally, to derive the efficiency for gamma rays, a numerical integration was performed in which the production of electron-positron pairs by photons was calculated for different depths of the 0.206-inch converter. Then the probability that an electron be produced with an energy E at the depth x in the converter was multiplied by the experimentally derived probability for the recording of a count from an electron of energy E that has to penetrate (0.206-x) inches of Pb before entering the telescope.

The result of this determination is indicated in Fig. 18. From the accumulated errors introduced into the problem it is felt that about ± 10% accuracy ought to be attached to the absolute value; however, the shape of the curve is believed to be more precisely determined.

D. Background and Subtraction

1. Background

Since the cross section for the reaction studied was quite low, particularly careful attention had to be given to possible sources of background.

There are two essentially different causes of spurious counts in the gamma telescope; multiple accidental coincidences of the kind to cause the electronics to respond as to a gamma ray, and gamma rays having their origin in other than proton-proton collisions.

To eliminate the first kind of background a manifold coincidence requirement was used, parts of which had resolving times of the order of a few millimicroseconds. Experimental checks were

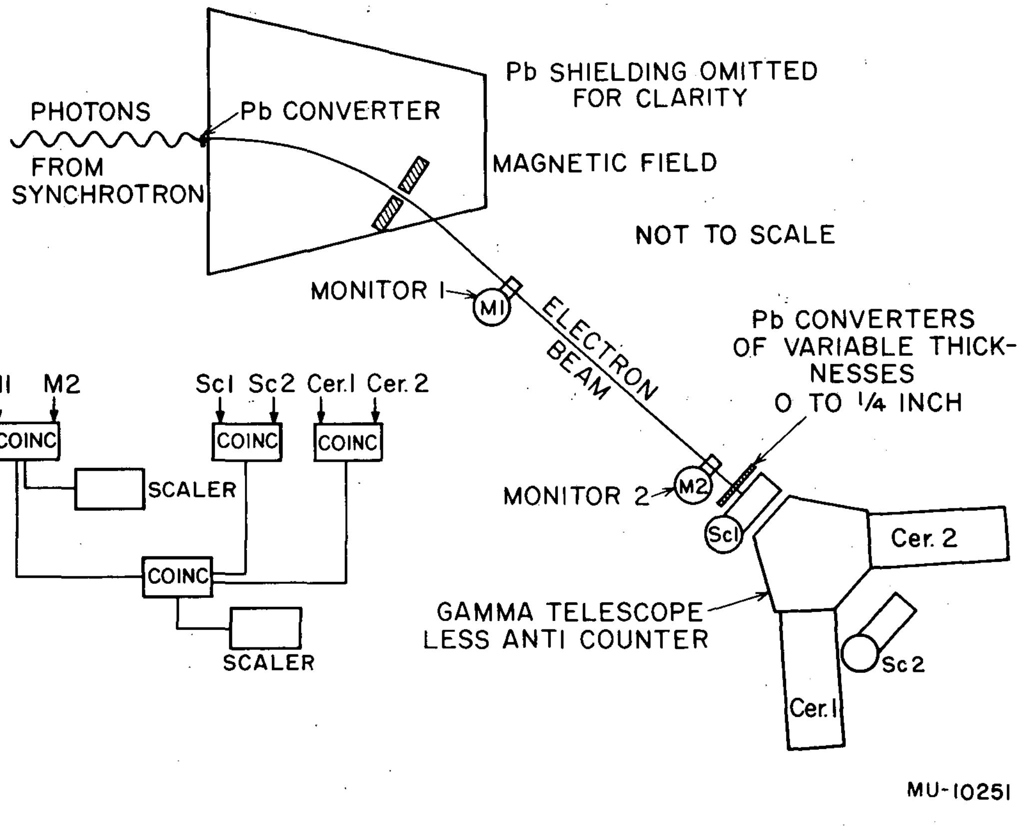

Fig. 16. Experimental arrangement for the determinations of the penetration of electrons through various thicknesses of lead and the counter telescope.

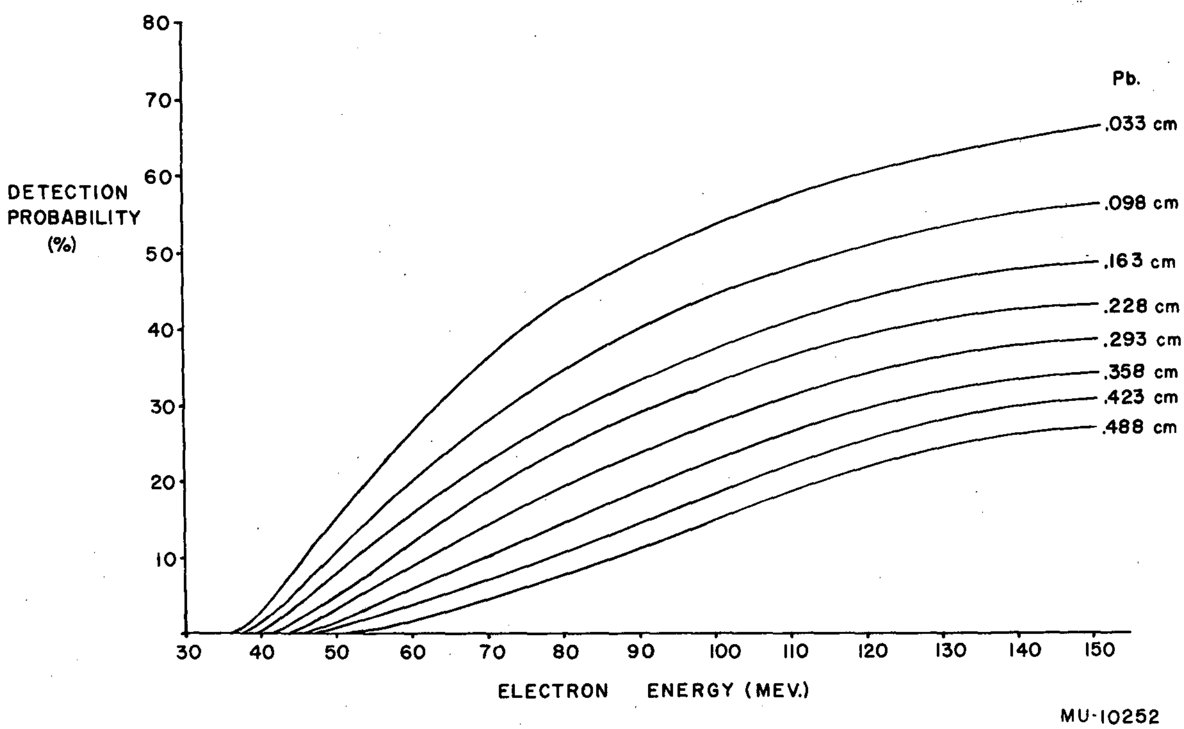

Fig. 17. Probabilities for electrons of various energies to penetrate several thicknesses of lead and to traverse the gamma-ray telescope (without the anti counter), and thus to register as a count.

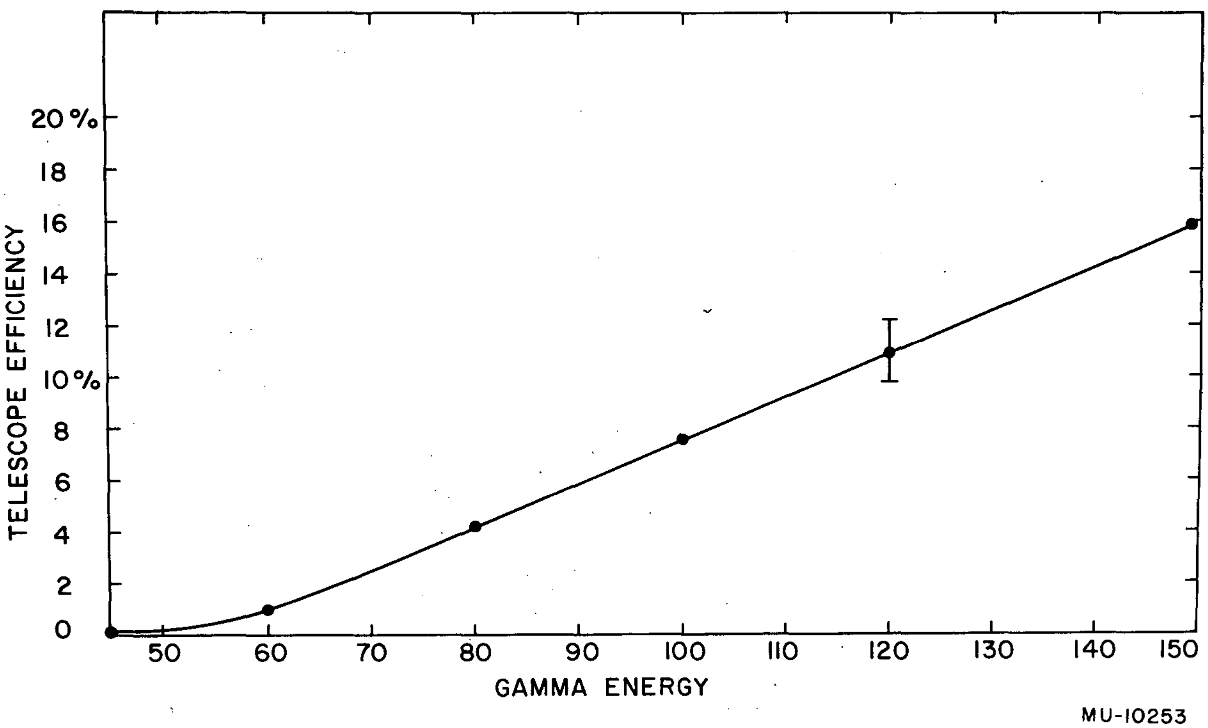

Fig. 18. Efficiency of the telescope for the detection of gamma rays of various energies.

made for these accidentals. It was possible to demonstrate that a variation in the intensity of the proton beam by a factor of 8 did not alter the counting rate per incident proton. The electronics would have responded to accidentals as approximately the cube of the beam level, so this provided a sensitive test. Further, blocking the channel in the collimation with lead reduced the counting rate to zero.

The second kind of background might arise from a number of different kinds of events. Admitting a "spray" of neutrons from the brass collimation, and the possibility of some protons' being outside the beam pattern at the telescope entrance window, we have the following possibilities:

a. π^o production by neutrons on the air behind the target, in the target walls, the collimation, etc.

b. π^o production by stray protons on the target walls, collimation, etc.

c. π^o production by protons in the beam on the deuterium "contamination" in the liquid hydrogen.

d. π^o production by protons multiply scattered from the beam into the target walls.

e. π^- capture in the liquid hydrogen, the π^- mesons coming from protons striking the carbon nuclei in the target entrance windows. The capture[19] leads to $\pi^- + p \rightarrow n + \gamma$ or $\pi^- + p \rightarrow n + \pi^o$.

A large number of other possible sources of background were eliminated by the design of the telescope. Electrons, charged mesons, or protons incident on the array were rejected by the anticounter, which was made to 100% efficiency for the detection of minimum ionization particles. Neutrons, by making charge-exchange or ordinary scatterings, could eject protons that could cause counts in Sc 1 and Sc 2, but not in the Cerenkov counter. By capture in lead, neutrons can give 8-Mev gamma rays which can be detected in the Cerenkov counter, but by virtue of the approximately 40-Mev threshold of the telescope, these could not cause a count in the Sc 1 - Cer - Sc 2 combination.

The possible sources were dealt with as follows:

a. All neutron-induced events were subtracted by a process to be outlined below.

b. Stray proton production is similarly subtracted.

c. The normal deuterium content of hydrogen is 1 part in 7000. Hales and Moyer[20] report that the deuterium cross section relative to carbon is 0.14 ± .03. The carbon cross section is reported as 1.5 mb, giving a deuterium cross section of ~0.2 mb. This is about 20 times the cross section for hydrogen as reported by Mather and Martinelli (0.01 ± .03 mb).[14] Thus the contribution from this source is $\overline{20/7000}$; about 0.3%.

d. $\overline{\Theta^2}$ for the scattering of protons by liquid hydrogen in the path length of 50 cm is about 5×10^{-5} radians^2 ($P\,\Theta\, d\Theta \cong 55\, e^{-\Theta^2/10^{-4}}$). The minimum angle of scatter that can bring a beam proton into the target walls in the area of the sensitive region is ~0.1 radian. The probability of such a scattering is:

$$P(.1)\, d\Theta \sim 55\, e^{-(.1)^2/10^{-4}} \sim 55\, e^{-100}.$$

Since the cross section/cm^2 for π^0 production in the walls is less than 10 times that in hydrogen, the total probability for a proton to scatter and produce a π^0 from the styrofoam is of the order of $(55\, e^{-100}) \times 10 \times 50$ cm (50 cm is the length of wall seen by the telescope). This will be entirely negligible.

e. The surface density of the entrance window of the target is 0.175 g/cm^2. The material is polystyrene, which consists principally of carbon (C_8H_7). The carbon cross section[21] for π^- production at 0° to the beam, integrated over the energy range (27 → 39 Mev) of mesons that can stop in the sensitive region of the target, is 6×10^{-30} cm^2/steradian. Since this sensitive region lies some 11 inches from the entrance window, the solid angle subtended is of the order of 0.3 steradian. The effective cross section is thus about 2 microbarns. Taking the Mather and Martinelli value quoted above for the proton cross section, and considering the relative numbers of nuclei contained in the target window and the sensitive hydrogen volume (1.33 g/cm^2) we obtain the ratio:

$$\frac{\pi^0 \text{ events from } \pi^- \text{ capture}}{\pi^0 \text{ events from p-p production}} \cong \frac{2 \times 10^{-30} \times (0.175\ \text{g/cm}^2)/(12\text{g/mole C})}{10^{-29} \times (1.33\ \text{g/cm}^2)/(1\text{gm/mole H})} \sim 0.2\%.$$

This will be a source of background; however, the effect will be masked by the counting statistics in this experiment.

2. Subtraction

The subtraction procedure used was the following:

Run	Target Contained	Beam*
A	Liquid Hydrogen (LH_2)	deflected*
B	Gaseous (STP) hydrogen (GH_2)	deflected
C	LH_2	undeflected*
D	GH_2	undeflected

Let us adopt the notation that "P on LH" means protons incident on liquid hydrogen, "N on air" means neutrons incident on air behind the target but within the field of view of the telescope, etc. We can then list the sources of counts in the four runs as the following:

Run No. A.
a. P on LH_2
b. P (stray) on target walls, collimation, etc.
c. N on LH_2
d. N on target walls, collimation, etc.

Run No. B
a. P on GH_2
b. P (stray) on target walls, collimation, etc.
c. N on GH_2
d. N on target walls, collimation, etc.

Run No. C
a. (<u>no</u> P on LH_2)
b. P on air behind target
c. N on LH_2
d. N on target walls, collimation, etc.

Run No. D
a. (<u>No</u> P on GH_2)
b. P on air behind target
c. N on GH_2
d. N on target walls, collimation, etc.

If we then subtract Run B from Run A, we get:

$$(A-B) = (P \text{ on } LH) - (P \text{ on } GH) + (N \text{ on } LH) - (N \text{ on } GH).$$

Subtracting Run D from Run C yields

$$(C-D) = (N \text{ on } LH) - (N \text{ on } GH).$$

---

* The magnet in the cave could be alternately turned on or off; it was thus possible to steer the proton beam into the target, or to allow it to pass, undeflected, beside the target.

Subtracting (C-D) from (A-B), we have for the net counting rate those events due to (P on LH) - (P on GH). We ignore the contribution of P on GH because of the relative densities of gaseous (STP) hydrogen and liquid hydrogen.

It is this final counting rate which is used as data.

E. Meson Decay: Spectra

The neutral meson lives about 10^{-15} second, decaying into two oppositely directed photons in its own rest frame, each of which has an energy equal to half the meson rest mass. When viewed from a frame other than the meson rest frame, these photons may appear with Doppler-shifted energies and with the 180° angle of emission altered by aberration. In this experiment, where the mesons are created near threshold, the meson generally has some velocity with respect to the center-of-momentum frame of the colliding protons. In addition, this c. m. frame is moving in the laboratory system with a velocity dependent upon the initial kinetic energy of the incident proton.

For an isotropic c. m. distribution of neutral mesons, the photon emission (in the c. m. frame) is isotropic, although there is an energy spread, which is greater for higher meson velocities.

If, however, the mesons are emitted in the P-state with a $\cos^2\theta$ contribution, there tends to be another kind of photon distribution. Where the meson has zero velocity, the photon distribution must be isotropic, but as the meson velocity increases, the distribution tends to take on the $\cos^2\theta$ shape. In addition, the spectrum develops an energy spread. This can be seen in the limiting case of very high velocities, with β approximately 1, where the aberration of the photons is so great that they appear to go in almost the same direction as the originating meson, much as a high-energy photon from an electron bremsstrahlung moves in almost the same direction as the incident electron.

The meson velocities dealt with in this experiment are low and only a mild modification of the spherical distribution is achieved; nevertheless, it is sufficient to be detectable.

The derivation of the photon spectrum due to decaying mesons having a velocity β_o in the center-of-momentum frame and viewed by an observer in the laboratory system where the c.m. velocity is β is carried out in Appendix VII-A and summarized here, in the formula:

$$I(\vartheta, k_L)d\Omega_L dk_L =$$
$$(\beta_o\gamma_o k'')^{-1}\sum_n a_n P_n\left(\frac{\cos\vartheta-\beta}{1-\beta\cos\vartheta}\right)P_n\left(\frac{1}{\beta_o}\left[1-\frac{k''}{\gamma_o\gamma k_L(1-\beta\cos\vartheta)}\right]\right)\frac{d\Omega_L dk_L}{\gamma(1-\beta\cos\vartheta)},$$

where:

$k'' = M\pi^o C^2/2$,

β_o = c.m. meson velocity $\div$ C,

$\gamma_o = (1 - \beta_o^2)^{-1/2}$,

β = (vel. of c.m.) $\div$ C,

$\gamma = (1 - \beta^2)^{-1/2}$,

ϑ = observer's angle of view in lab system with respect to proton beam,

k_L = photon laboratory energy,

$d\Omega_L$ = observer's (lab) solid angle.

(Meson distribution expanded as $N(\theta') = \sum_n a_n P_n(\cos\theta')$.)

The spectra resulting from spherically symmetric meson production, and a $\cos^2\theta$ variation in intensity, for various values of the meson energy in the center-of-momentum frame, but viewed at the constant laboratory angle of 67°, or 135°, are plotted in Fig. 19.

F. Solid Angles and Transmission Factor

The average solid angle subtended by the telescope from the target region was computed as the average of the solid angles subtended from various parts of the target. These were:

$\overline{\Delta\Omega}$ (@ 67°) = 0.00223 steradian,

$\overline{\Delta\Omega}$ (@ 135°) = 0.00231 steradian.

Inserted into the collimation channel was an 8-inch-long block of Be. This served to attenuate by dE/dx any charged particles incident upon it. A certain small fraction of the incident gammas was also converted by it and subsequently rejected by the "anticounter." We define a "transmission factor" as the fraction of gammas that get through the Be, as well as through one-half the anticounter without conversion. This factor is Tr = 0.85, and is assumed to be independent of the photon energy.

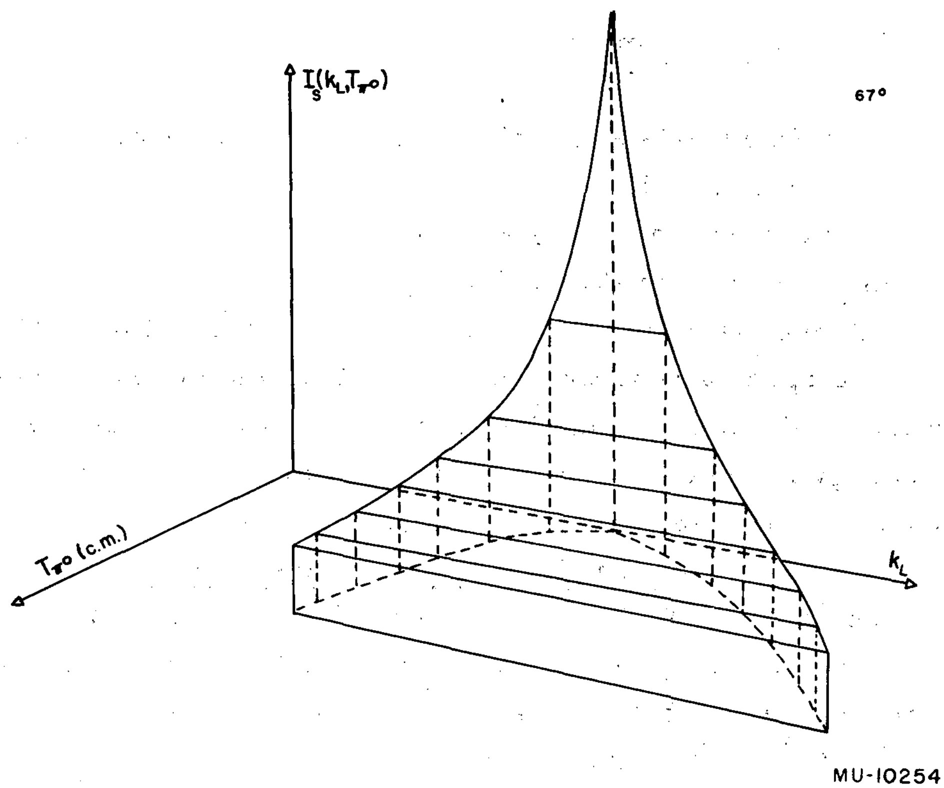

Fig. 19a. Spectral intensity of gamma rays in the laboratory system for the lab viewing angle 67°, resulting from the decay of a π^0 created with isotropic symmetry and energy T_π in the c.m. system, plotted from $T_\pi = 0$ to T_π = kinematic maximum.

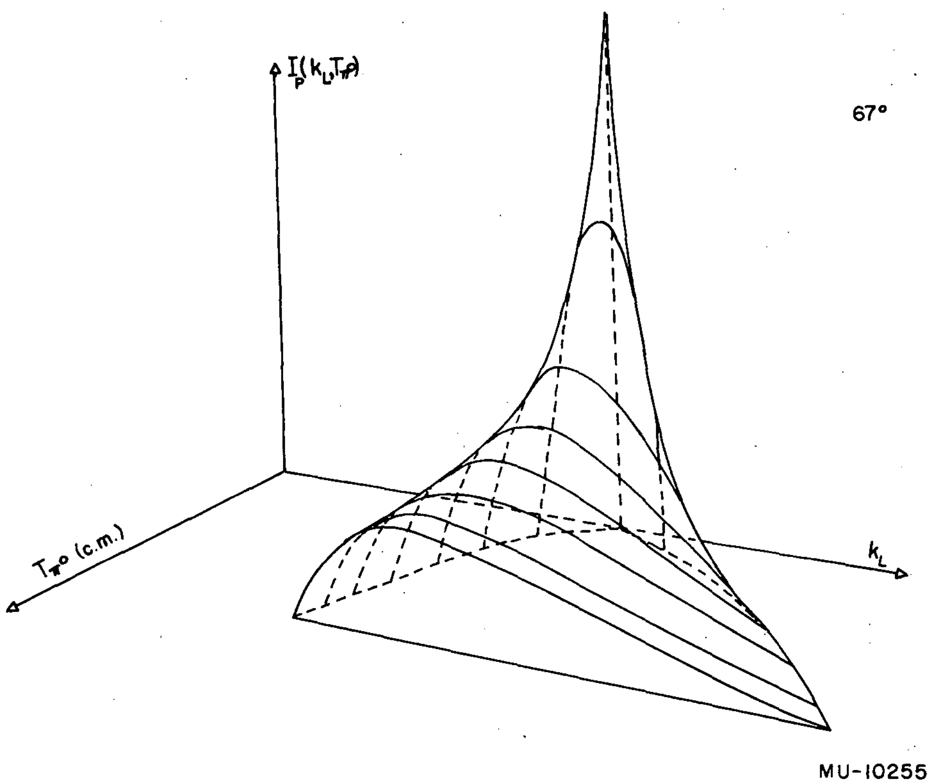

Fig. 19b. Same case as 19a except that π^0 is created with a $\cos^2\theta$ distribution in the c.m. system.

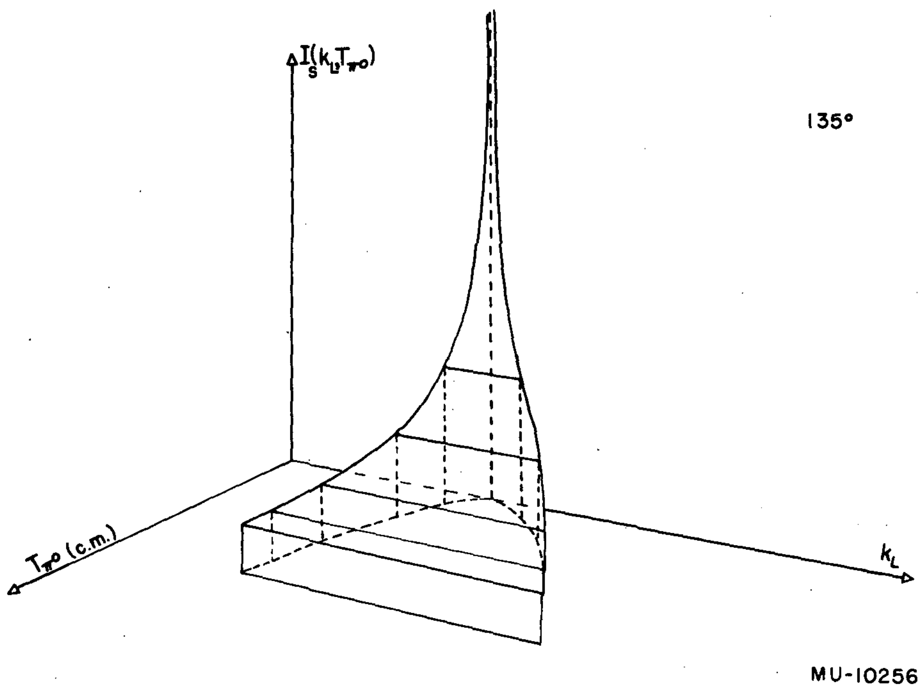

Fig. 19c. Same case as 19a except that the lab observation angle is 135°.

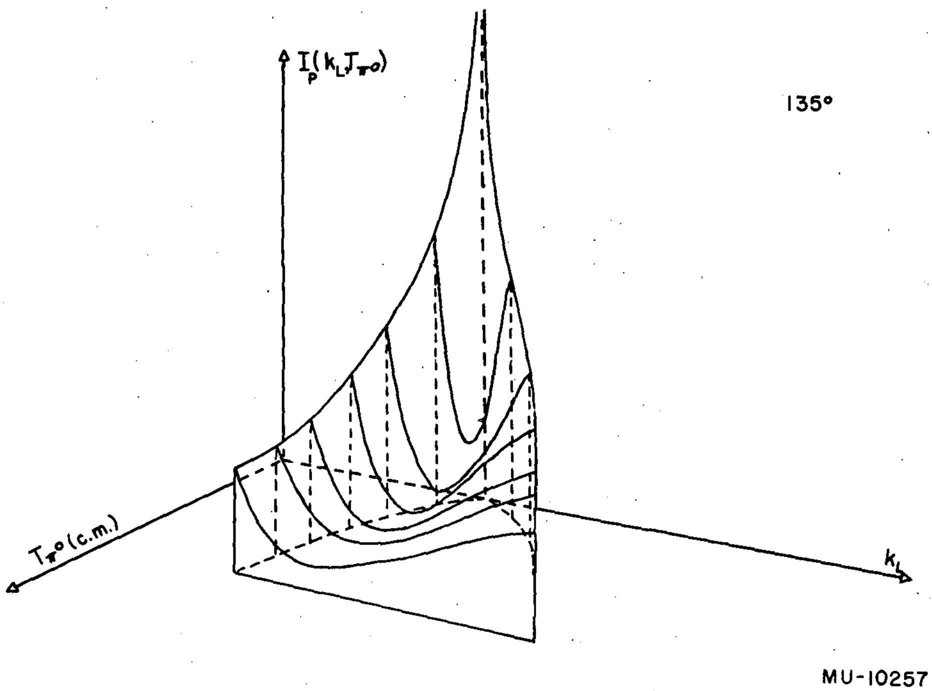

Fig. 19d. Same case as 19b except that the lab observation angle is 135°.

G. Folding Operations and Calculation of Cross Sections

For a given proton bombarding energy, mesons may be created that have energies ranging all the way from zero to some kinematically determined maximum. For the apparatus described here, high-velocity mesons are detected more effectively than low-velocity ones by virtue of the Doppler shifting of the gammas into higher-energy regions where the telescope is a more efficient detector. For this reason, an analysis of the data requires some knowledge of the relative numbers of mesons created with different velocities.

The theoretical treatment of meson production as done by Gell-Mann and Watson[2] and by others (Section II, Theory) gives specific predictions for meson energy spectra for the S and P states.

As an example, consider the case where the maximum meson energy is 24 Mev. There are 3 "classes" of meson production contributing to the cross section, each with a different energy spectrum. If we normalize to 1 meson, we have:

Class Ss $(\sigma \propto \eta_o^2)$: $\frac{dn(Ss)}{dT_{\pi o}} = \frac{2}{\pi T_o} \sqrt{\frac{T_{\pi o}}{T_o - T_{\pi o}}}$; $T_o = 24$ Mev

Class Pp $(\sigma \propto \eta_o^8)$: $\frac{dn(Pp)}{dT_{\pi o}} = \frac{128}{3\pi T_o^4} \quad T_{\pi o}^{3/2}(T_o - T_{\pi o})^{3/2}$; $T_o = 24$ Mev

Class Ps $(\sigma \propto \eta_o^6)$: $\frac{dn(Ps)}{dT_{\pi o}} = \frac{16}{\pi T_o^3} \quad T_{\pi o}^{1/2}(T_o - T_{\pi o})^{3/2}$; $T_o = 24$ Mev.

These three populations are plotted in Fig. 20.

If we write the total meson-production cross section in terms of the three contributions of momentum dependence, for a particular bombarding energy giving η_o maximum momentum, we have

$\sigma(\eta_o) = a_{Ss}\,\eta_o^2 + a_{Ps}\,\eta_o^6 + a_{Pp}(C+1)\,\eta_o^8$, where C is the variable introduced in the Pp angular distribution. The number of counts registered by the telescope, per incident proton, then becomes (see Appendix B):

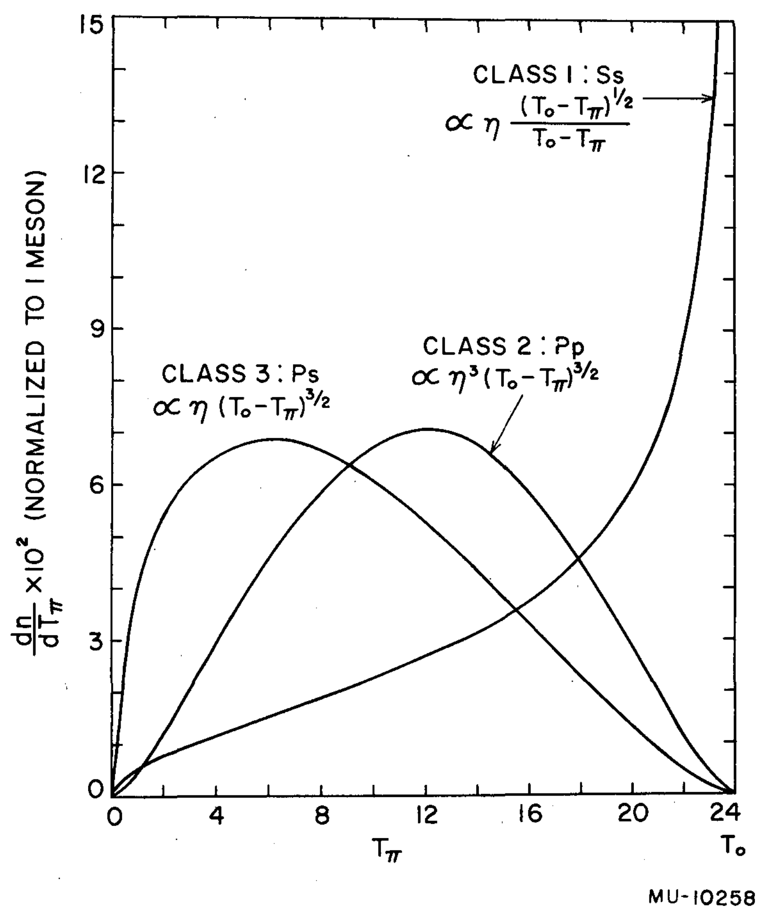

Fig. 20. Probability for a meson to be produced with energy $T_\pi \rightarrow T_\pi + dT_\pi$, where T_o is the maximum attainable energy, for the three classes of production: Pp, Ps, Ss.

$$C_1(\eta_o) =$$

$$N_1 \Delta\Omega_1 \mathrm{Tr}\Big[a_{Ss}\eta_o^2 \int_{T_\pi}\int_{k_L} I_S(T_{P_1}, T_\pi, \vartheta, k_L)\,\epsilon(k_L)\,\frac{dn(Ss)}{dT_\pi}\,dk_L\,dT_\pi +$$

$$a_{Ps}\eta_o^6 \int_{T_\pi}\int_{k_L} I_S(T_{P_1}, T_\pi, \vartheta, k_L)\,\epsilon(k_L)\,\frac{dn(Ps)}{dT_\pi}\,dk_L\,dT_\pi +$$

$$a_{Pp}\eta_o^8 \Big\{C \int_{T_\pi}\int_{k_L} I_S(T_{P_1}, T_\pi, \vartheta, k_L)\,\epsilon(k_L)\,\frac{dn(Pp)}{dT_\pi}\,dk_L\,dT_\pi +$$

$$\int_{T_\pi}\int_{k_L} I_P(T_{P_1}, T_\pi, \vartheta, k_L)\,\epsilon(k_L)\,\frac{dn(Pp)}{dT_\pi}\,dk_L\,dT_\pi \Big\}\Big]$$

where T_π is integrated from $T_\pi=0$ to T_π=maximum meson energy(c.m.).

k_L is integrated from minimum to maximum gamma ray energy (Lab.)

and N_1 = number of protons/cm^2 for Run 1,

$\Delta\Omega_1$ = average solid angle for Run 1,

Tr = transmission factor,

$I_S(T_{P_1}, T_\pi, \vartheta, k_L)$ = spectral intensity of gamma rays in the laboratory system, for the lab viewing angle ϑ and bombarding energy T_{P_1}, resulting from the decay of a π^o created with isotropic symmetry and energy T_π in the c.m.

$I_P(T_P, T_\pi, \vartheta, k_L)$ = spectral intensity of gamma rays in the laboratory system, for the lab viewing angle ϑ and bombarding energy T_{P_1}, resulting from the decay of a π^o created with a $\cos^2\theta'$ angular distribution and energy T_π in the c.m.

$\epsilon(k_L)$ = efficiency for the detection of gammas of energy k_L by the telescope.

Since there are four experimental points, there are four equations such as this: one for the angle 135^o, and one for each of the three different bombarding energies at 67^o. If we designate the integrals by F_1 through F_{16}, we can write:

$$C_1 = N_1 \Delta\Omega_1 \mathrm{Tr}\left[a_{Ss}\eta_{01}^{2} F_1 + a_{Ps}\eta_{01}^{6} F_2 + C\, a_{Pp}\eta_{01}^{8} F_3 + a_{Pp}\,\eta_{01}^{8} F_4\right],$$

$$C_2 = N_1 \Delta\Omega_1 \mathrm{Tr}\left[a_{Ss}\eta_{02}^{2} F_5 + a_{Ps}\eta_{02}^{6} F_6 + C\, a_{Pp}\eta_{02}^{8} F_7 + a_{Pp}\,\eta_{02}^{8} F_8\right],$$

$$C_3 = N_1 \Delta\Omega_1 \mathrm{Tr}\left[a_{Ss}\,\eta_{03}^{3} F_9 + a_{Ps}\eta_{03}^{6} F_{10} + C\, a_{Pp}\eta_{03}^{8} F_{11} + a_{Pp}\eta_{03}^{8} F_{12}\right],$$

$$C_4 = N_2 \Delta\Omega_2 \mathrm{Tr}\left[a_{Ss}\,\eta_{01}^{2} F_{13} + a_{Ps}\eta_{01}^{6} F_{14} + C\, a_{Pp}\eta_{01}^{8} F_{15} + a_{Pp}\eta_{01}^{8} F_{16}\right].$$

Because the only unknowns are the a_{Ss}, a_{Ps}, a_{Pp} and Ca_{Pp} this is a set of four linear equations in four unknowns. We have solved these by standard methods to arrive at the values given below. The errors that have been attached are from the statistical indeterminancy of the data.

The values are:

$$a_{Ss} = 0.020 \pm .010 \text{ mb},$$

$$a_{Ps} = 0.084 \pm .11 \text{ mb};$$

$$C a_{Pp} = 0.081 \pm .21 \text{ mb};$$

$$a_{Pp} = 0.57 \pm .11 \text{ mb}.$$

Here a_{Ps}, $C\,a_{Pp}$ are equal to zero within the statistical spread shown. Further, the contributions from these terms are small for small values of η_o, and small in comparison with a_{Pp} where η_o is large. They are included in the statistical spread of the final cross section.

VI RESULTS

A. Cross Section Versus Energy

The total cross section for π^o production, near threshold, expressed as a function of the kinematic maximum possible meson momentum divided by μc, is a sum of two terms:

$$\sigma_{11}(\text{mb}) = 0.020\ \eta_o^{\ 2} + 0.57\ \eta_o^{\ 8} \left\{ \begin{array}{l} +\sqrt{(.01\ \eta_o^{\ 2})^2 + (.11\ \eta_o^{\ 6})^2 + (.31\ \eta_o^{\ 8})^2} \\ -\sqrt{(.01\ \eta_o^{\ 2})^2 + (.11\ \eta_o^{\ 8})^2} \end{array} \right.$$

This function is plotted in Fig. 21. The terms α_{Ps}, $C\,\alpha_{Pp}$ are possibly not zero, and serve in this figure to make the two statistical limits unequal.

B. Angular Distribution

The α_{Ss}, α_{Ps}, $C\,\alpha_{Pp}$ contribute mesons having an isotropic distribution, while the term in α_{Pp} contributes mesons having a $\cos^2\theta$ distribution. Including the possibility that α_{Ps}, $C\,\alpha_{Pp}$ are not zero, within the statistical errors attached, we have for the angular distribution:

$$\frac{d\sigma_{11}(\text{mb})}{d\Omega} = \frac{1}{4\pi} \left[.020\ \eta_o^{\ 2} \left\{ \begin{array}{l} +\sqrt{(.01\ \eta_o^{\ 2})^2 + (.11\ \eta_o^{\ 6})^2 + (.21\ \eta_o^{\ 8})^2} \\ -\ .010\ \eta_o^{\ 2} \end{array} \right. \right] +$$

$$\frac{3}{4\pi} \left[.57 \pm .11 \right] \eta_o^{\ 8} \cos^2\theta .$$

If we express this as

$$\frac{d\sigma}{d\Omega} = A + B\ \cos^2\theta$$

we can plot the ratio A/B versus η_o. This is done in Fig. 22.

At very low energies, isotropic production dominates. At a value of η_o of about 0.5 the spherically symmetric and $\cos^2\theta$ production are equal, and for higher energies the $\cos^2\theta$ production rapidly becomes the dominant term.

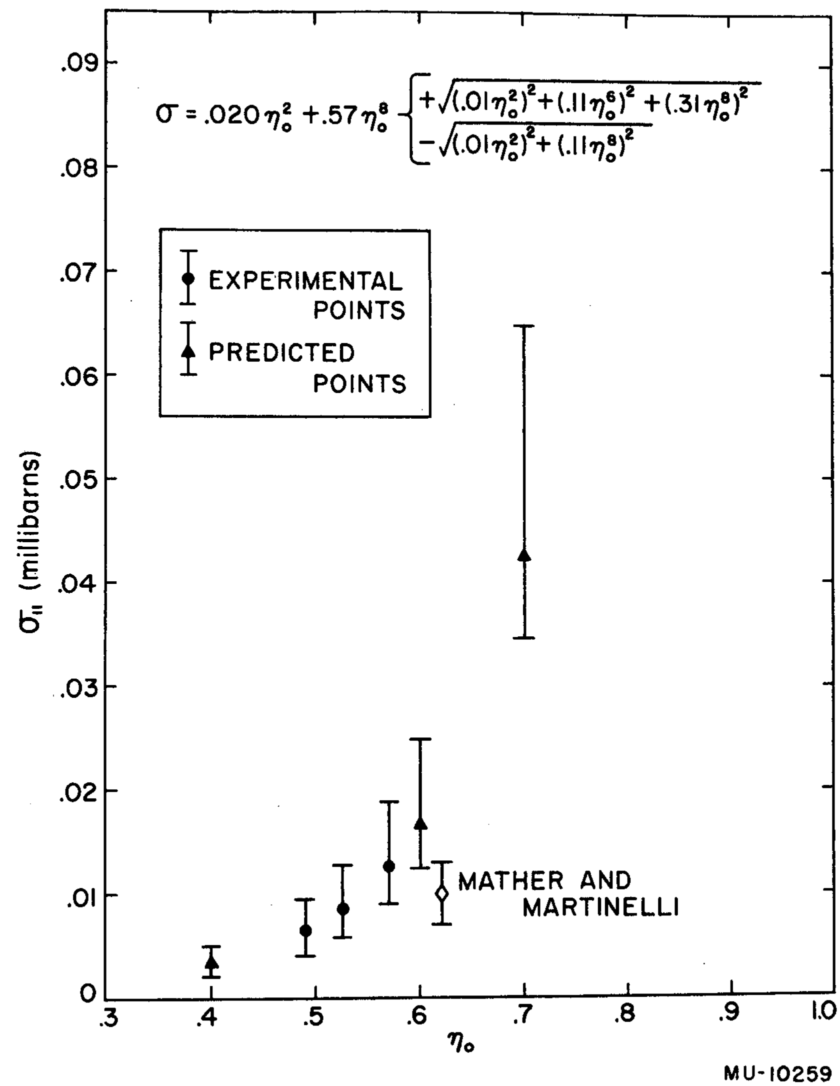

Fig. 21. Cross section for π^0 production in proton-proton collisions as a function of maximum meson momentum in units of μc.

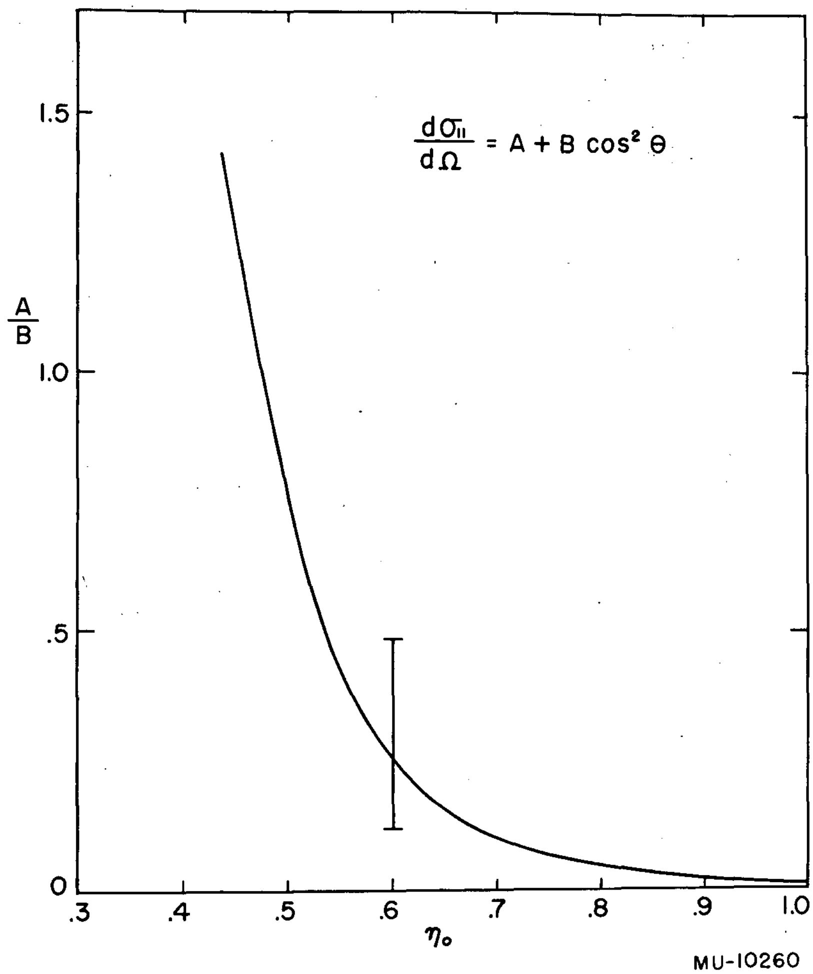

Fig. 22. Ratio of the spherical to $\cos^2\theta$ contributions to the cross section as a function of η_o.

C. Comparison with Other Experiments

This process, because of experimental difficulties, has not been extensively investigated. Mather and Martinelli[14] measured the total cross section at 337 Mev and found the value

$$\sigma_{11} = 0.010 \pm .003 \times 10^{-27}\ \text{cm}^2.$$

This is plotted on Fig. 21 and can be seen to lie close to the predicted curve of this experiment.

Marshall and Marshall[13] have reported a value at the energy 430 Mev,

$$\sigma_{11} = 0.45 \pm .15 \times 10^{27}\ \text{cm}^2.$$

Extrapolating the curve of Fig. 21 to this region gives a prediction that is about three times too large. This is indicated in Fig. 23. This disagreement is not unreasonable. The energy, 430 Mev, is well above threshold and some of the assumptions that were made for this experiment are no longer valid. In particular, one might expect that the matrix elements might not be independent of energy over such a large range. It is expected that the $\eta_o^{\,8}$ dependence is modified for higher energies, otherwise the cross section becomes unreasonably large.

Tyapkin et al.[22] have reported a value for the total cross section at 670 Mev

$$\sigma = 3.7 \pm .8 \times 10^{-27}\ \text{cm}^2,$$

and point out that this shows a dependence on momentum between 480 and 670 Mev of $\eta_o^{\,4.5}$.

D. Summary and Extensions

The total cross section and the angular distribution of mesons produced in the process

$$P + P \rightarrow \pi^o + P + P,\ \ \sigma_{11}$$

has been measured at three energies close to threshold. At proton bombarding energy such that the maximum meson momentum in the center-of-mass system is 0.47 the spherically symmetric production term in the cross section is equal to the $\cos^2\theta$ term. Above this energy, the $\cos^2\theta$ term dominates and rapidly becomes much larger.

This experiment offers evidence that the p-state production of mesons is a strong selection rule. For η_o=0.5, there is only 13 Mev

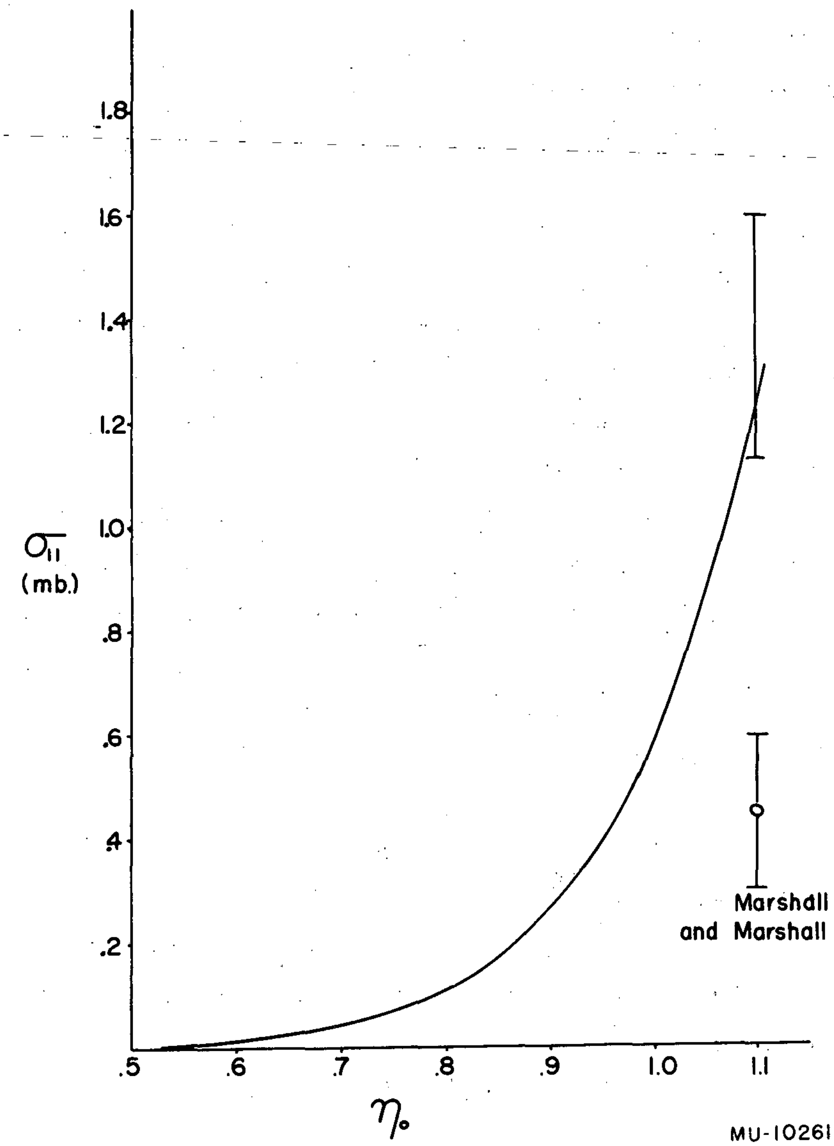

Fig. 23. Extrapolation of the excitation function and comparison with the datum of Marshall and Marshall.

available to be shared by the nucleons and the meson. Hence, class Ss is energetically much preferred. Since the class Pp production is observed to equal the Ss production, one may conclude that the production of mesons into the p-state is a much more likely event than the production into an s-state.

The rapid rise in cross section with energy, as the Pp state becomes more effective, gives the cross section an effective dependence proportional to η_o^8 above η_o equal to about 1. It is expected that this will be modified with increasing energy. The measurement of the actual form of the cross section versus energy for the energy range 360 Mev and above would constitute an interesting experiment.

APPENDIX

A. Calculation of Photon Spectra

Although the neutral mesons created in the collisions may have a unique angular distribution, their decay products, photons, will tend to duplicate this distribution only weakly, for the higher the meson velocity the stronger the correlation between the two shapes. To calculate the energy spectrum and intensity distribution of photons due to meson production with various angular distributions and velocities is the purpose of this appendix. The resultant spectra, computed for the observer's fixed laboratory angle of 67° and 135°, are presented in Fig. 19.

Select a coordinate system with its origin at the center of momentum of the colliding protons, with its Z axis towards the observer (in the c.m. frame), and with the line of motion of the protons in the X-Z plane. The angle between the proton line and the Z axis is the observer's c.m. angle of view.

If we then have an arbitrary direction, its spherical coordinates are θ, ϕ. Let the angle between this arbitrary direction and the proton line of motion be designated θ'. This is illustrated in Fig. 24.

Because there is no preferred azimuthal direction in the proton-proton collision, it can be assumed that the meson production will be axially symmetric. The meson intensity as a function of angle will therefore depend only on θ' and, for generality, this function will be assumed to be expanded in a series of Legendre polynomials,

$$N(\theta') = \sum_n a_n P_n(\cos \theta'), \qquad (1)$$

where this is normalized to one meson. (θ' is the correct variable since it is the polar angle in a coordinate system where the proton line is the Z axis.)

One has now to get from this expression in θ' to an expression for the intensity of meson production as a function of θ, ϕ. The general solution to the problem of transforming a Legendre polynomial, expressed in terms of the polar angle from some arbitrary axis having

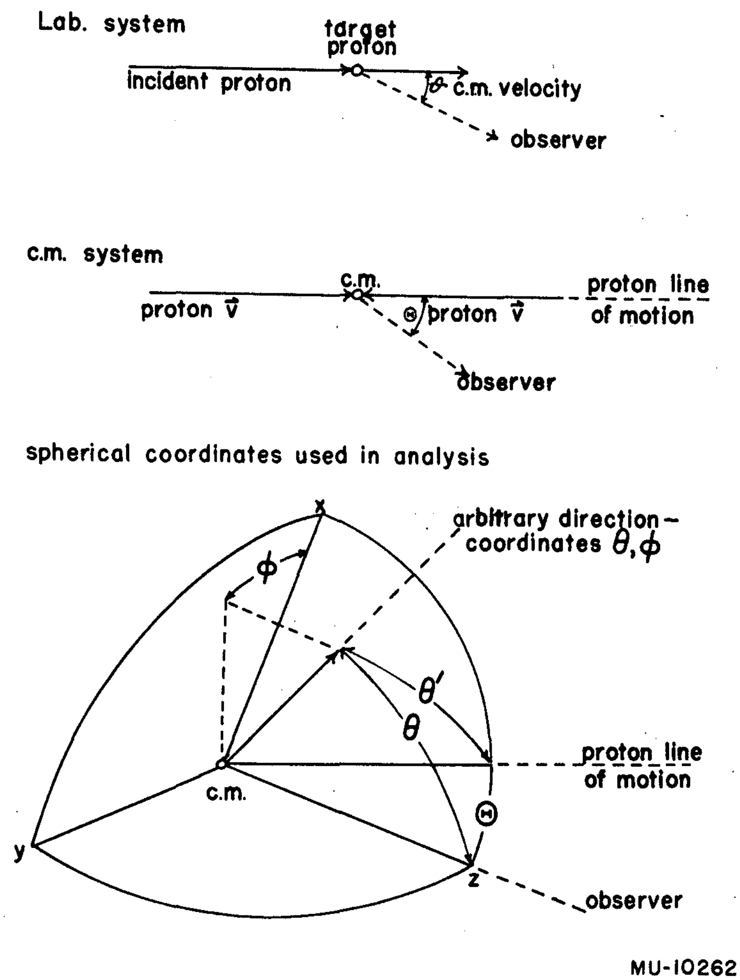

Fig. 24. Coordinate systems for the proton-proton collisions, and spherical coordinates used in the analysis of the meson production and decay.

coordinates Θ, 0 in a θ, ϕ system, is solved by the theory of biaxial harmonics.[23] The following expression is found to hold:

$$P_n(\cos\theta') = \sum_{m=0}^{n} (2-\delta_m^o) \frac{(n-m)!}{(n+m)!} P_n^m(\cos\Theta)\, P_n^m(\cos\theta) \cos m\phi. \qquad (2)$$

If we substitute this for $P_n(\theta')$ in Eq. (1), we find

$$N(\theta,\phi) = \sum_n a_n \sum_m (2-\delta_m^o) \frac{(n-m)!}{(n+m)!} P_n^m(\cos\Theta)\, P_n^m(\cos\theta) \cos m\phi, \qquad (3)$$

which gives the meson intensity per steradian at the spherical coordinate point θ, ϕ. If we multiply this by the element of solid angle, we have

$$N(\theta,\phi)\, d\,\Omega = N(\theta,\phi)\, d(-\cos\theta)\, d\,\phi. \qquad (4)$$

Concentrating our attention on those mesons produced at the angle θ, we see that for their decay gammas to be emitted into $\theta = 0$, and observed, these gammas must be emitted at the angle θ with respect to the meson velocity.

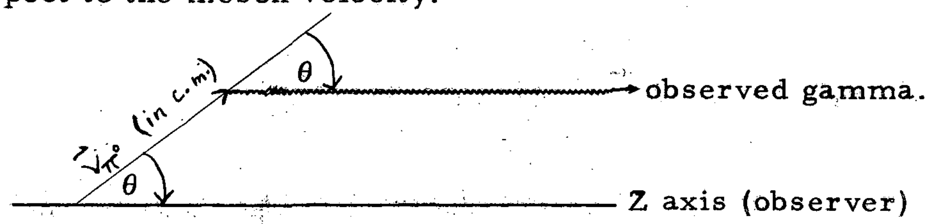

This angle θ uniquely determines the character of Doppler shift and aberration of the gamma from the π^o rest frame to the c.m. frame, as well as the solid angle factors that enter. So interest really centers on the number of mesons created at the angle θ for any ϕ angle whatsoever. We therefore integrate over the range of ϕ:

$$N(\theta)\, d(-\cos\theta) = \sum_n a_n \sum_m (2-\delta_n^o) \text{ ------ } \int \cos m\phi\, d\phi \qquad (5)$$

$$= 2\pi \sum a_n P_n(\cos\Theta)\, P_n\ (\cos\theta)\, d(-\cos\theta). \qquad (6)$$

In the π^o rest frame, the two-photon gamma decay is isotropic. Introducing a double-prime notation to distinguish this frame, we have for the (fractional) number of gammas emitted into the solid angle $d\Omega''$:

$$dn = 2 \cdot \frac{d\Omega''}{4\pi} \quad ; \quad \frac{dn}{d\Omega''} = \frac{1}{2\pi} . \tag{7}$$

In the c.m. frame we have

$$dn = \frac{dn}{d\Omega''} \frac{d\Omega''}{d\Omega_c} \Delta\Omega_c = \frac{1}{2\pi} \frac{d(-\cos\theta'')}{d(-\cos\theta)_c} \Delta\Omega_c , \tag{8}$$

where $\Delta\Omega_c$ is the solid angle subtended by the observer.

The relativistic transformation laws yield the following expression for the aberration of photons:

$$\cos\theta'' = \frac{\cos\theta - \beta_o}{1 - \beta_o \cos\theta} ,$$

$$\text{where } \beta_o = \frac{v_\pi \text{ (in cm.)}}{C} \tag{9}$$

Therefore

$$\frac{d(\cos\theta'')}{d(\cos\theta)} = \frac{1}{\gamma_o^2 (1 - \beta_o \cos\theta)^2} . \tag{10}$$

Thus dn, the fractional number of photons emitted into solid angle $\Delta\Omega_c$ is

$$dn = \frac{1}{2\pi} \frac{\Delta\Omega_c}{\gamma_o^2 (1 - \beta_o \cos\theta)^2} \tag{11}$$

To finally derive the total gamma intensity $I(\theta)$, we multiply this number (of photons per meson) by the number of mesons produced in the interval $\theta \to \theta + d\theta$:

$$I(\theta)\, d(-\cos\theta)\, \Delta\Omega_c = 2\pi \sum a_n P_n(\cos \Theta)\, P_n(\cos\theta) \frac{d(-\cos\theta)\, \Delta\Omega_c}{2\pi\, \gamma_o^2 (1 - \beta_o \cos\theta)^2} . \tag{12}$$

The variation of the angle of emission, $\theta \to \theta + d\theta$, introduces a variation of the photon energy of $k \to k + dk$, which can be derived from the relativistic expression

$$k = \frac{k''}{\gamma_o (1 - \beta_o \cos\theta)} , \tag{13}$$

where k'' is the photon energy in the meson frame and is equal to 67 Mev. Differentiating, we get

$$dk = \beta_o k'' \, d(-\cos\theta)/\gamma_o(1-\beta_o\cos\theta)^2 \quad , \tag{14}$$

which yields, upon inversion,

$$d(-\cos\theta) = \frac{\gamma_o(1-\beta_o\cos\theta)^2}{\beta_o k''} \, dk. \tag{15}$$

If we also solve Eq. (13) for the k dependence of $\cos\theta$, we get

$$\cos\theta = \left(\frac{1}{\beta_o} - \frac{k''}{\beta_o\gamma_o k} \right). \tag{16}$$

Substituting Eqs. (15) and (16) into Eq. (12), we get

$$I(k)dk\,\Delta\Omega_c = (\beta_o\gamma_o k'')^{-1} \sum_n a_n P_n(\cos \Theta) P_n\left(\frac{1}{\beta_o} - \frac{k''}{\beta_o\gamma_o k}\right) dk\Delta\Omega_c. \tag{17}$$

Equation (17), giving the spectral intensity in the c. m. -system variables, may be expressed in terms of the laboratory-system variables by the following transformation. We are observing photons emitted at the (c. m.) angle Θ with respect to the motion of the c. m. in the laboratory system.

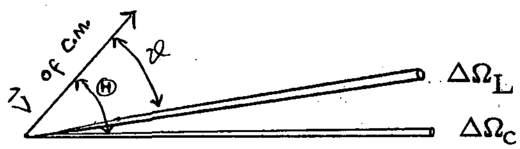

The c. m. angle Θ will undergo aberration to the lab angle ϑ, the energy k of the photon will be Doppler-shifted to the lab energy k_L, and the solid angle $\Delta\Omega_c$ will be changed to $\Delta\Omega_L$, by the motion of the c. m. The following relations hold:

$$\cos\Theta = \frac{\cos\vartheta - \beta}{1 - \beta\cos\vartheta} \quad , \tag{18}$$

$$\Delta\Omega_c = \frac{1}{\gamma^2(1-\beta\cos\vartheta)^2} \, \Delta\Omega_L, \tag{19}$$

$$dk = \gamma(1-\beta\cos\vartheta)dk_L. \tag{20}$$

For a transformation of variables we have:

If $x = g(\xi)$, and $y = h(\eta)$,

then $f(x, y)dx\, dy = f(g(\xi), h(\eta))\ J\left(\frac{x, y}{\xi, n}\right) d\xi\, dy$, (21)

where J is the Jacobian of the transformation.

For this case,

$$J\left(\frac{\Omega_c,\ k}{\Omega_L,\ k_L}\right) = \frac{\gamma(1-\beta\cos\vartheta)}{\gamma^2(1-\beta\cos\vartheta)^2} \quad . \tag{22}$$

Writing Eq. (17) with these changes, we have

$I(k_L)dk_L\Delta\Omega_c =$

$$(\beta_o\gamma_o k'')^{-1} \sum_n a_n P_n\left(\frac{\cos\vartheta-\beta}{1-\beta\cos\vartheta}\right) P_n\left(\frac{1}{\beta_o}\left[1-\frac{k''}{\gamma_o\gamma k_L(1-\beta\cos\vartheta)}\right]\right)\frac{dk_L\Delta\Omega_c}{\gamma(1-\beta\cos\vartheta)}. \tag{23}$$

May have error !! Corr

This is the final expression for the spectral intensity emitted at the angle ϑ(lab) for π^os having an angular distribution expressed as $\sum a_n P_n(\cos\theta')$ and a velocity β_o in the c. m. system, which in turn has a velocity β with respect to the laboratory system.

Two specific cases are important.

1. "S" state production -- spherical symmetry:

$$a_o = \frac{1}{4\pi},\ a_n=0,\ n \neq 0;$$

$$I_S(T_P, T_\pi, k, \vartheta)dk_L\Delta\Omega_c = \frac{1}{4\pi\beta_o\gamma_o k''} \cdot \frac{\Delta\Omega_c\, dk_L}{\gamma(1-\beta\cos\vartheta)} \ . \tag{24}$$

2. $\cos^2\theta'$ production

$$a_o = \frac{1}{4\pi},\ a_2 = \frac{2}{4\pi},\ a_n = 0,\ n \neq 0, 2.$$

$$(N(\theta') = \frac{3}{4\pi}\cos^2\theta')$$

$I_p(T_p, T_\pi, k_L, \vartheta)dk_L\ \Delta\Omega_c =$

$$\frac{3}{8\pi}\left(\frac{1}{\beta_o\gamma_o k''}\right)\left(\frac{1}{\gamma(1-\beta\cos\vartheta)}\right) \cdot \left\{\ E\ \right\}\ dk_L\Delta\Omega_c \tag{25}$$

where $\left\{ E \right\} =$

$$\left\{ 1 - \left(\frac{\cos\vartheta - \beta}{1-\beta\cos\vartheta} \right)^2 + \left[3\left(\frac{\cos\vartheta-\beta}{1-\beta\cos\vartheta} \right)^2 - 1 \right] \frac{1}{\beta_o{}^2} \left[1 - \frac{k''}{\gamma_o \gamma k_L (1-\beta\cos\vartheta)} \right]^2 \right\}$$

B. Calculation of Cross Sections

At a given bombarding energy there is a kinematically determined maximum velocity possible for the meson. The c.m. gamma spectrum emitted by a π^o will be a function of that velocity. As indicated in Section II, the probability of a meson's having an energy $T_\pi \to T_\pi + dT_\pi$ is a function of T_π and of the class of production of the meson. The spectrum therefore is a function of the production class, and through the spectrum the detection probability is a function of the class.

For example, given that the maximum meson momentum is η_{01} for a bombarding energy T_1, then the photon spectrum per incident proton per N protons per cm^2 per steradian at the laboratory angle ϑ is

$$I(k_L)dk_L d\Omega =$$

$$N\left[a_{Ss}\,\eta_o{}^2 \int_{T_\pi=0}^{T_\pi=\max} I_s(T_1, T_\pi, k_L, \vartheta)\,\frac{dn(Ss)}{dT_\pi}\,dT_\pi \; + \right.$$

$$a_{Ps}\,\eta_o{}^6 \int_{T_\pi=0}^{T_\pi=\max} I_s(T_1, T_\pi, k_L, \vartheta)\,\frac{dn(Ps)}{dT_\pi}\,dT_\pi \; +$$

$$a_{Pp}\,\eta_o{}^8 \left\{ C \int_{T_\pi=0}^{T_\pi\max} I_s(T_1, T_\pi, k_L, \vartheta)\,\frac{dn(Pp)}{dT_\pi}dT_\pi \; + \right.$$

$$\left. \left. \int_{T_\pi=0}^{T_\pi\max} I_p(T_1, T_\pi, k_L, \vartheta)\,\frac{dn(Pp)}{dT_\pi}\,dT_\pi \right\} \right] dk_L\, d\,\Omega,$$

where I_s and I_p are the spectra for spherical and $\cos^2\theta$ meson production respectively.

The use of a detecting apparatus that detects gammas of all energies, although with a varying efficiency, $\epsilon(k_L)$ dependent upon the gamma energy, causes the actual detection probability to be proportional to an integral of this spectrum.

Detection probability $\propto \int I(k_L)\,\epsilon(k_L)\,dk_L$, so per incident proton, the counting rate will be

$$C_1(\eta_o) =$$

$$N_1 \Delta\Omega_1 \mathrm{Tr} \Bigg[a_{Ss}\eta_o^2 \int_{T_\pi}\int_{k_L} I_s(T_{p_1}, T_\pi, \vartheta, k_L)\,\epsilon(k_L)\,\frac{dn(Ss)}{dT_\pi}\,dk_L\,dT_\pi +$$

$$a_{Ps}\eta_o^6 \int_{T_\pi}\int_{k_L} I_s(T_{p_1}, T_\pi, \vartheta, k_L)\,\epsilon(k_L)\,\frac{dn(Ps)}{dT_\pi}\,dk_L\,dT_\pi +$$

$$a_{Pp}\eta_o^8 \Bigg\{ C \int_{T_\pi}\int_{k_L} I_s(T_{p_1}, T_\pi, \vartheta, k_L)\,\epsilon(k_L)\,\frac{dn(Pp)}{dT_\pi}\,dk_L\,dT_\pi +$$

$$\int_{T_\pi}\int_{k_L} I_p(T_{p_1}, T_\pi, \vartheta, k_L)\,\epsilon(k_L)\,\frac{dn(Pp)}{dT_\pi}\,dk_L\,dT_\pi \Bigg\} \Bigg]$$

where N_1 = number of protons/cm^2,

$\Delta\Omega_1$ = solid angle of telescope,

Tr = transmission of gammas into telescope.

Because the I_s and I_p are in general complicated functions of their variables, the integrals were calculated by numerical integration. For each integral the spectral intensity "I" was calculated at 24 different points. Each of these values was multiplied by the appropriate efficiency $\epsilon(k_L)$ for detection of that energy, by dn/dT appropriate to the production class, and by the intervals Δk_L, ΔT_π. A summation of these 24 terms then yielded the total probability for detection of the particular production class at the proton energy involved. An examination of the spectra plotted in Fig. 19 will show that the value of $I(k_L)$ changes slowly enough for the above to be a good averaging process.

A cross section at one proton energy and angle involves four integrals and the four experimental cases involve 16 integrals. If these are designated F_1 through F_{16}, we can write:

$$C_1 = N_1 \Delta\Omega_1 \, \mathrm{Tr} \left[a_{Ss} \eta_{01}^{2} F_1 + a_{Ps} \eta_{01}^{6} F_2 + C a_{Pp} \eta_{01}^{8} F_3 + a_{Pp} \eta_{01}^{8} F_4 \right],$$

$$C_2 = N_1 \Delta\Omega_1 \, \mathrm{Tr} \left[a_{Ss} \eta_{02}^{2} F_5 + a_{Ps} \eta_{02}^{6} F_6 + C a_{Pp} \eta_{02}^{8} F_7 + a_{Pp} \eta_{02}^{8} F_8 \right],$$

$$C_3 = N_1 \Delta\Omega_1 \, \mathrm{Tr} \left[a_{Ss} \eta_{03}^{2} F_9 + a_{Ps} \eta_{03}^{6} F_{10} + C a_{Pp} \eta_{03}^{8} F_{11} + a_{Pp} \eta_{03}^{8} F_{12} \right],$$

$$C_4 = N_2 \Delta\Omega_2 \, \mathrm{Tr} \left[a_{Ss} \eta_{01}^{2} F_{13} + a_{Ps} \eta_{01}^{6} F_{14} + C a_{Pp} \eta_{01}^{8} F_{15} + a_{Pp} \eta_{01}^{8} F_{16} \right].$$

Since C_1 through C_4 are the experimental quantities, we have four equations in the four unknown, the a_{Ss}, a_{Ps}, a_{Pp} and $C\,a_{Pp}$.

ACKNOWLEDGMENTS

It is a pleasure to express my sincerest appreciation to Professor Burton Moyer who introduced me to the field of meson physics and who suggested this problem. His help, inspiration, and encouragement were freely given at all times.

I wish to extend my gratitude to the many other persons whose work and ideas contributed to the experiment. Special mention is due John Osher and Robert Cence for the particularly large part they played in the development and operation, respectively, of the instrumentation.

A special thanks goes also to James Vale and the crews of the cyclotron for their excellent operation of this machine.

This work was done under the auspices of the U. S. Atomic Energy Commission.

BIBLIOGRAPHY

1. A. H. Rosenfeld, Phys. Rev. 96, 139 (1954).
2. Gell-Mann and Watson, Annual Rev. Nuc. Sci. (Ann. Rev. Inc) 4, 219 (1954).
3. R. H. Hildebrand, Phys. Rev. 89, 1090 (1953).
4. R. A. Schluter, Phys. Rev. 95, 639(A) (1954).
5. Bjorklund, Crandall, Moyer, and York, Phys. Rev. 77, 213 (1950).
6. Steinberger, Panofsky, and Steller, Phys. Rev. 78, 802 (1950).
7. Panofsky, Aamodt, Hadley, Phys. Rev. 81, 565, (1951).
8. Breuckner, Serber, and Watson, Phys. Rev. 81, 575 (1951).
9. K. A. Breuckner, Phys. Rev. 82, 598 (1951).
10. Chew, Goldberger, Steinberger, and Yang, Phys. Rev. 84, 58 (1951).
11. K. M Watson and K. A. Breuckner, Phys. Rev. 83, 1 (1951).
12. K. M. Watson, Phys. Rev. 88, 1136 (1952).
13. J. Marshall and L. Marshall, Phys. Rev. 88, 632 (1952).
14. J. W. Mather, and E. A. Martinelli, Phys. Rev. 92, 780 (1953).
15. L. I. Schiff, Quantum Mechanics, New York, McGraw-Hill 1949 1st ed. p 265.
16. Richard Madey, "A Fast Counting System for High-Energy Particle Measurements," University of California Radiation Laboratory Report No. UCRL-1880.
17. Marvin Rich and Richard Madey, "Range-Energy Tables," University of California Radiation Laboratory Report No. UCRL-2301, March 1954.
18. R. Mather and E. Segrè, Phys. Rev. 84, 191 (1951).
19. Panofsky, Aamodt, and Hadley, Phys. Rev. 81, 565 (1951).
20. Hales and B. J. Moyer, Phys. Rev. 89, 1047 (1953).
21. Walter F. Dudziak, "Production Cross Sections for Positive and Negative Pions from Carbon Initiated by 340-Mev Protons"(thesis) University of California Radiation Laboratory Report No. UCRL-2564, Apr. 1954.
22. A. A. Tyapkin, M. S. Kosodaev, and YuD. Prokoshkin, Doklady Akademii Nauk USSR 100, No. 4, 689 (1955).
23. W. R. Smythe, Static and Dynamic Electricity, New York, McGraw-Hill, p 154 (1950).